Utrecht University
Faculty of Geosciences

MSc Thesis

MSc Earth, Structure and Dynamics

2DV numerical simulations of turbidites in ponded basins: Insights from depositional patterns

Author:
J.H.C. Ooms[1]
Student number: 3752194

Supervisors:
J.T. Eggenhuisen[1]
D.-J. Walstra[2,3]
J.E.A. Storms[3]
H. Van der Vegt[3]

[1]Utrecht University
[2]Deltares
[3]TUDelft

April 24, 2017

Abstract

A coarsening upward signature is expected for turbidites in ponded basins based on the fill-and-spill model. However, this model might be to simplistic. This study aims to identify how grain size composition and sill height affect the depositional patterns of turbidites within a 2DV ponded basin. A numerical modelling approach is adopted here and the open source software Delft3D is used to create a 2DV model of a ponded basin on a continental slope. A dataset of 15 model series was created to assess the influence of both initial composition and sill height of the ponded basin on the depositional patterns. Each series consisted of 4 or 5 surge-type turbidity current events. The presence of more cohesive material in the initial sediment composition results in larger amounts of erosion and larger currents. Two contradictory trends in grain size with decreasing sill height are observed. At the temporal and spatial scale of individual turbidites, a fining upward stacking pattern is found in the deposits. This is attributed to autogenic coarsening of the substrate. At the temporal and spatial scale of lobes or lobe complexes, the effects of flow stripping in a fill-and-spill basin are recognizable in the depositional characteristics of the turbidites. The contradiction between the two temporal and spatial scales illustrates that at a larger scale, the main autogenic process of coarsening of the substrate on the slope is counteracted by constant background sedimentation or changes in allogenic processes. These processes are put forward as controls on the recurrence interval of self-accelerating turbidity currents. Due to the displayed sensitivity of turbidity currents to changes in substrate erodibility, continued research regarding the influence of cohesive material and consolidation on turbidity current - bed interaction is recommended.

Keywords: turbidity currents, numerical modelling, ponded basin, depositional patterns, substrate erodibility.

Contents

1 Introduction

Turbidity currents are the main mode of distribution and deposition of sand in deep-sea settings (Weimer and Slatt, 2007a). Their deposits on the sea floor generally represent the final location of sediment in a source-to-sink system. Turbidity currents have been studied by means of seismic, core, and outcrop studies of their deposits, present-day observations (Xu, 2010; Hughes Clarke, 2016), laboratory experiments (e.g., Baas et al., 2004; Cartigny et al., 2013; de Leeuw et al., 2016) and numerical simulations (e.g., Blanchette et al., 2005; Abd El-Gawad et al., 2012; Basani et al., 2014; Bolla Pittaluga and Imran, 2014). Numerical simulations or process based modelling can provide the link between the data obtained from laboratory experiments on flow dynamics of turbidity currents (limited by scaling issues) and the stratigraphic properties of turbidity deposits as are observed from outcrop, core and seismic studies (Basani et al., 2014).

In an unrestricted basin-plain setting, the thickness and grain size of individual turbidites decrease away from their source as the turbidity current decelerates due to expansion and deposition (Middleton, 1967; Scheidegger and Potter, 1971; Garcia, 1994). The shape of the depositional lobes is dependent on composition of the system, with sand-rich systems leading to more channelized lobes and mud-rich systems to more sheet-like lobes (Weimer and Slatt, 2007b; Reading and Richards, 1994). It is thus apparent that composition of the turbidity current is an important parameter that influences the resulting geometry of the deposit.

In addition, complex sea floor topography will affect the depositional patterns of the turbidity current. Ponded basins, or mini-basins, are relatively small depressions on the sea floor. Their geometry can be related to differential sediment compaction, faulting or diapiric movement of salt or mud (Brunt et al., 2004). Numerous of such ponded basins related to salt withdrawal have been documented on the continental slope in the northern Gulf of Mexico (Winker, 1996). A coarsening upward fill-and-spill signature of turbidite deposits within the ponded basin is expected, based on progressively reducing sill height and increasing amounts of overspill (e.g., Brunt et al., 2004). However, the fill-and-spill model has proven unable to explain the chronology of the stratigraphic infill of the Brazos-Trinity slope system, consisting of four linked mini-basins (Beaubouef and Friedmann, 2000; Mallarino et al., 2006; Prather et al., 2012). Here a forward process model approach is adopted to test the fill-and-spill concept.

The turbidite deposit in the (ponded) basin reflects the interactions of both allogenic processes (e.g. eustasy, climatic conditions, tectonic activity) and autogenic processes (sediment gravity-flow processes and development of depositional relief) (Romans et al., 2009). Autogenic processes reflect the dynamics between the current and the sediment bed. The bed material plays a key role in the development of the turbidity current (Sequeiros et al., 2009). It may determine whether a current will self-accelerate and deposit sediment in the ponded basin, or whether a current will merely wane and deposit all its sediment before it reaches the ponded basin. Allogenic processes affect the type and amount of sediment supply available for reworking by turbidity currents and may influence the transition from waning to self-accelerating turbidity currents.

This study aims to identify how grain size composition and sill height affect the resulting depositional patterns and characteristics of turbidites within a ponded basin. A numerical modelling approach is adopted here and the open source software Delft3D is used. Delft3D is a modelling framework that is mainly used for understanding and predicting hydrodynamics and morphodynamics in deltaic, coastal, river, lake and estuarine areas. It has been used, among other things, to study sediment transport models (Hu et al., 2009), effects of sediment properties on morphology in deltaic settings (e.g., Geleynse et al., 2011; Caldwell and Edmonds, 2014; van der Vegt et al., 2016) and riverine settings (van Maren, 2007; Schuurman et al., 2013). The software has previously

been used to model turbidity currents in the Shihmen reservoir in Taiwan (Commandeur, 2015), but has not yet been applied to turbidity currents in the larger, continental slope - ocean floor scale of this study. Furthermore, no attempt has been made to study the stratigraphy of the resulting turbidites.

Five model series with different bathymetric profiles were created for each of three different initial sediment compositions, which leads to a total of 15 model series. One series consists of 4 or 5 turbidity current events in order to create a stacking pattern of turbidite beds. These bathymetries represent a varying sill height of the ponded basin. No allogenic controls are included, to assess only the autogenic processes that influence the created stacking patterns.

In this paper, first, the 2DV model setup is described in detail. Subsequently, the results of the 15 model series are described in terms of characteristic hydrodynamics and depositional patterns (basin wide as well as through synthetic wells). Finally, the results are discussed and used to show how the identified processes influence the depositional patterns in ponded.

2 Model setup

2.1 Delft3D-FLOW

The Delft3D software consists of several modules. For the simulations conducted here, the Delft3D-FLOW module is used, to simulate hydrodynamics, morphology changes and sediment transport. Sediment transport formulations have been validated thoroughly by Lesser et al. (2004) and references therein. The hydrodynamics are based on 3D Navier-Stokes equations for an incompressible fluid (Deltares, 2016). The aspect ratio between depth and horizontal length scale is small (see Section 2.2.1). Therefore the use of the shallow water equations is valid and the vertical momentum equation is reduced to a hydrostatic pressure relation. Furthermore, the Boussinesq approximation is applied, meaning that the effect of variable density is only considered in the pressure term and otherwise neglected. This greatly simplifies the governing equations computed by the model.

For more detailed description of the governing equations and the numerical implementation of these equations, the reader is referred to Deltares (2016) and references therein.

2.2 2DV model setup

2.2.1 Model geometry

A depth-averaged horizontal (2DH) approach is not able to capture the interaction between the sediment bed and the 3D flow structures (Meiburg and Kneller, 2010). Therefore, a 2DV approach is adopted here, which is able to capture heterogeneities in the vertical plane. The model is set up along two dimensions in the vertical plane and the third dimension is only 1 grid cell wide. The horizontal resolution of the grid cells is 200 m by 200 m. The resulting domain has a total length of 150 km and a width of 0.2 km (Figure 1). The bathymetric profiles of the simulations represent the transition from continental slope with a ponded basin to ocean floor (Figure 2). In the vertical direction the grid is divided in 80 layers, specified as a percentage of the total water depth. This percentage is smallest at the bottom (0.03 %), where the best resolution is required to model the hydrodynamics of the turbidity current in sufficient detail. At the water surface, where negligible influence of the turbidity current on the hydrodynamics is expected, the percentage is largest (7.18 %). With a maximum water depth of 1800 m, these layer thicknesses translate to less than 0.54 m thick at the bottom up to 129 m thick at the water surface. Maximum depth at the ponded basin is only 800 m. This translates to layer thicknesses of 0.24 m and 57 m at bottom and surface respectively.

With a horizontal grid resolution of 200 m, the aspect ratio between depth and horizontal length scale for the lower layers is sufficiently small for the shallow water assumption to be valid in each grid cell. Vertical fluxes between grid cells will be dominated by eddy viscosity and not by advection (Deltares, 2016). For the coarsest layers at the top of the model, this as-

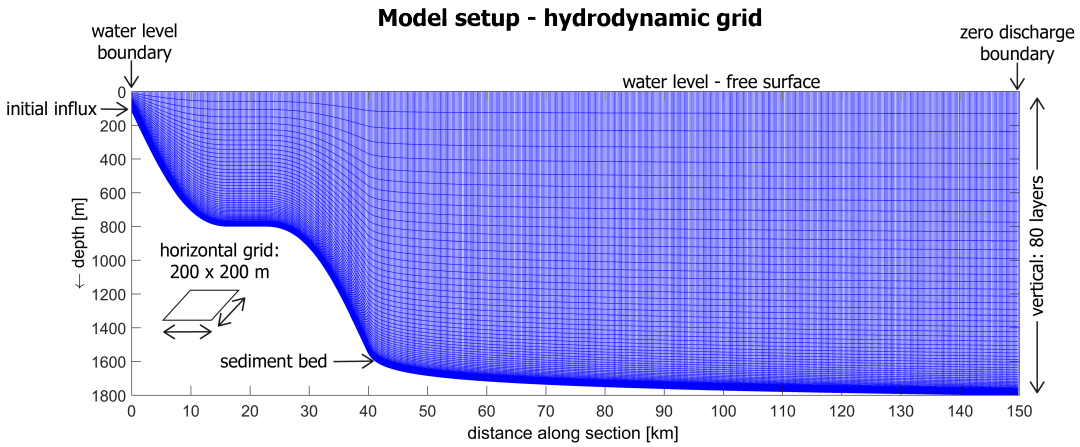

Figure 1: An overview of the model geometry and boundary conditions used is presented. The Hydrodynamic grid of the model is shown in blue. See text for further details.

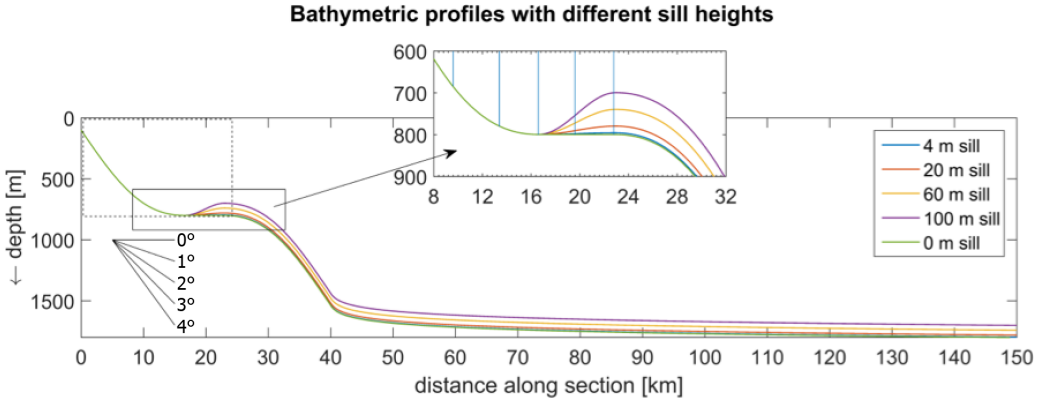

Figure 2: The five different initial bathymetric profiles used in the experiments are shown. The different profiles have different sill heights, ranging from 0 m to 100 m, and represent different amounts of confinement of the ponded basin. The streaked box indicates the cropped area of figures 6 and 7. The inset figure gives a more detailed image of the different sill heights. The vertical blue lines in the inset figure give locations of the vertical wells shown in Figure 12.

sumption might not be appropriate where water depths are relatively large compared to the horizontal length scale (aspect ratio up to 65 %). Yet in the case of a deep ambient fluid, as is the case in this model setup, the motion of the overlying fluid can be neglected and the shallow water assumption still holds (Meiburg and Kneller, 2010).

2.2.2 Boundary conditions

The upstream boundary condition is set to a constant water level of 0 m and an influx of sediment-laden water is imposed in the 47 lowest layers in the first grid cell, corresponding to the lowest 10 m of the water column. The influx of $2{\cdot}10^4$ m^3/s is evenly distributed. The influx lasts 10 minutes, with a specified sediment concentration (in kg/m^3). This is analogous to a surge type turbidity current, for example triggered by slope failure following an earthquake (Kneller and Buckee, 2000). An overview of the model geometry and boundary conditions setup can be found in Figure 1.

The downstream boundary of the model is a discharge boundary which is set to 0 m^3/s for model stability. The closing of the downstream boundary leads to a return flow in the

upper domain of the model. The reflection parameter alpha (RPA) can be varied from zero to 10.000 to make the boundaries less reflective for short wave disturbances that originate from inside the model (Deltares, 2016). Here the RPA is set to 200 s^2 for both boundaries, to prevent oscillations in the water level to reflect from the downstream boundary and to amplify towards the upstream boundary where the water depth becomes significantly shallower. Due to the large dimensions of the model domain and the use of the RPA, the return flow will have a negligible influence on the hydrodynamics and sediment transport in the turbidity current. Furthermore, the simulation will be ended before the head of the turbidity current reaches the downstream boundary of the model.

The bottom boundary conditions such as bottom roughness are dependent on the sediment bed and will differ locally. A free slip condition is applied to the side walls of the domain. The top boundary condition is defined as a free surface.

2.2.3 Time frame

The calculation time step of the simulations is set to 0.6 seconds. The model output is written to file every 5 simulated minutes to reduce computational time and the size of the output file. The total simulated time is 48 hours, where the block discharge is released from 30 to 40 minutes after the start of the model time.

2.2.4 Sediment and stratigraphy

Both cohesive and non-cohesive sediment classes are used to assess the influence of different initial sediment compositions on resulting depositional patterns. Five adjacent sediment classes (based on the Wentworth size class) are used, ranging from medium sand to medium silt. An overview of the parameters used to define each sediment class is given in Table 1. The non-cohesive sediment classes are defined by their D50, whereas the cohesive sediment classes are defined by their settling velocity and critical bed shear stresses for sedimentation and erosion. The D50 of the cohesive sediment classes is calculated from their settling velocity using Stokes' Law. The sediment transport formulas for non-cohesive and cohesive sediments used by the model are adopted from van Rijn (2007a,b,c) and Galappatti and Vreugdenhil (1985), respectively.

The initial stratigraphy of the model is built up of 15 $\times$ 1 m thick layers of equal composition (which composition see Section 2.3.1). The model calculates fluxes of erosion and deposition during each time step based on the near bed reference concentration of the different sediment classes (Lesser et al., 2004). These fluxes result in changes in composition as well as in quantity of the sediment stored in a transport layer with 30 cm thickness located directly under the bed level. The sediment in the transport layer is homogeneously mixed. When the sediment storage volume of the transport layer is exceeded, the surplus of sediment is stored in additional underlying layers (underlayers) of 10 cm thick each. When the sediment storage volume of the transport layer is not completely filled, sediment from the first underlayer is added to the transport layer, thereby effectively eroding the stored stratigraphy (Deltares, 2016). A maximum of 75 underlayers is defined, which represents 7.5 m of detailed stratigraphy. For models in which more than 7.5 m of additional stratigraphy is deposited, the number of underlayers in the model is increased to 150 to capture all deposited stratigraphy.

2.2.5 Bottom roughness

The formulation of bottom roughness length Z_0 [m] is preferred over the use of Chézy or Manning coefficient formulation since the latter formulations are strongly depended on the water depth as they include hydraulic radius. The water depth varies strongly in the continental slope - ocean floor setting of this model. Consequently, the dependence on water depth of the Chézy or Manning formulations will lead to large differences in bottom roughness with depth. This is thought to misrepresent the bottom roughness. The bottom roughness Z_0 is related to the geometric Nikuradse rough-

Table 1: The specifications of the different sediment classes as used in the models are shown. *D50 of the cohesive sediment classes is calculated from the settling velocity using Stokes' Law.

Sediment class	Sediment type	Specific density	Dry bed density	D50	Settling velocity	Critical bed shear stress for sedimentation	Critical bed shear stress for erosion	Erosion parameter
[-]	*[-]*	*[kg/m^3]*	*[kg/m^3]*	*[μm]*	*[m/s]*	*[N/m^2]*	*[N/m^2]*	*[kg/m^2/s]*
medium sand	non-cohesive	2650	1600	400	-	-	-	-
fine sand	non-cohesive	2650	1600	150	-	-	-	-
very fine sand	non-cohesive	2650	1600	90	-	-	-	-
coarse silt	cohesive	2650	500	36*	$4.8{\cdot}10^{-3}$	$1.0{\cdot}10^{3}$	$1.5{\cdot}10^{-1}$	$1.0{\cdot}10^{-4}$
medium silt	cohesive	2650	500	32*	$3.6{\cdot}10^{-3}$	$1.0{\cdot}10^{3}$	$1.2{\cdot}10^{-1}$	$1.0{\cdot}10^{-4}$

ness length scale k_s through $Z_0 = k_s/30$ (Nikuradse, 1933). Based on typical k_s values ranging from 0.15 m for rough river beds to 0.01 m for smooth surfaces with only ripples or similar type of roughness elements (Deltares, 2016), this implies Z_0 values of 0.005 m and 0.0003 m to be rough and smooth respectively. A uniform Z_0 value of 0.005 m is used to include not only effects of grain-scale roughness, but also effects of bedforms and other sorts of microtopography that are likely to be present in a 200 m by 200 m area of sea floor.

2.2.6 Turbulence

A κ-ϵ turbulence closure model is applied to solve turbulent scales at and below grid size resolution. It describes the transport of both the turbulent kinetic energy κ and energy dissipation ϵ. In addition, a background vertical eddy viscosity and background vertical eddy diffusivity of $1{\cdot}10^{-6}$ m^2/s are applied. These background values act as minimum values which affect the vertical mixing of sediment. For detailed information on formulation and implementation of the turbulence model the reader is referred to the Delft3D-FLOW manual (Deltares, 2016) and references therein.

2.2.7 Other settings

Other settings that differ from the default settings of the model input are discussed here. The constant water density is set to 1025 kg/m^3, which is the average density of sea water at the surface. This value is applied to the water in the initial influx as well. The water density does not change with depth in the model. Since the instantaneous interaction between input flow and the sediment bed is of interest in this study, the spin up interval before morphological changes take place, is set to 10 min. Furthermore, the effect of sediment on fluid density is included in the model, as it would influence the flow velocity and bed shear stress in the lower computational layers, especially if the $\kappa - \epsilon$ turbulence closure model is used (Deltares, 2016).

2.3 Simulations

Multiple series of simulations were conducted to constrain the influence of initial composition and effective sill height on the depositional patterns of the turbidity currents. Five model series with different bathymetric profiles were created for each of three different initial sediment compositions, leading to a total of 15 model series. One series consists of four to five turbidity current events. The resulting stratig-

Table 2: The relative volume percentages of each sediment class are shown for the three different grain size compositions; mud-rich, mixed and sand-rich. In the last row the mean grain size of each composition is shown.

Sediment class	Composition		
	mud-rich	mixed	sand-rich
medium sand	5 %	15 %	25 %
fine sand	10 %	15 %	25 %
very fine sand	15 %	20 %	25 %
coarse silt	35 %	25 %	15 %
medium silt	35 %	25 %	10 %
D50 [μm]	72	117	168

raphy and bathymetry after each event are used as initial conditions for the subsequent event. In this way, a stratigraphic stacking pattern of four to five turbidites was created per model series.

2.3.1 Grain size composition

Three different initial compositions are defined, based on their dominant sediment type; mud-rich, mixed and sand-rich. The distribution between the five different sediment classes (medium sand, fine sand, very fine sand, coarse silt and medium silt, presented in Table 1) for each initial composition is given in Table 2. The used initial composition is not only applied to the sediment composition present in the initial influx, but also to the sediment composition of the initial stratigraphy of the first run of each series.

2.3.2 Sill height

Five different initial bathymetries are used to simulate different amounts of confinement in the ponded basin. Zero sill height represents a flat ramp geometry with no confinement. The slope before the flat ramp (first slope) and the second slope that transitions into the ocean floor have the same geometries for all different bathymetries. The steepness of the slope ranges from 4° to 0° (Figure 2). The only difference between the bathymetries is the height of the sill between the two slopes. The sill height is defined as the vertical difference between the lowest part of the ponded basin and the top of the sill. For the series of models sill heights of 0 m, 4 m, 20 m, 60 m and 100 m are used (Figure 2). The horizontal scale of the ponded basin is in the order of 20 km. This falls within the range of scale from a few kilometres to tens of kilometres, as found for salt-withdrawal minibasins on the north slope of the Gulf of Mexico (e.g. Violet et al., 2005).

2.3.3 Concentration

For the mud-rich composition models events 1-4 all have 1.5 vol% initial influx sediment concentrations. In case of the mixed and sand-rich composition models, the first event has a 1.5 vol% initial influx sediment concentration and events 2-5 have 2.0 vol% concentrations. If the initial concentration is kept at 1.5 vol%, no turbidite stacking pattern in the ponded basin is created for the mixed and sand-rich models. The sediment load of the subsequent turbidity currents is deposited on the slope and does not reach the ponded basin. The increase in initial concentration is needed to produce a sequence of self-accelerating currents that deposits sediment within the ponded basin. The initial concentration of the mud-rich composition models is not increased to 2.0 vol%, since a concentration of 1.5 vol% was sufficient to create a turbidite stacking pattern in the ponded basin. With a specific density of 2650 kg/m^3 initial concentrations of 1.5 vol% and 2.0 vol% translate to a total amount of sediment per cubic meter of water of 39.75 kg/m^3 and 53.00 kg/m^3, respectively.

It is emphasized that these are the sediment concentrations of the initial influx, and not necessarily of the resulting turbidity current. Due to sediment exchange with the bed and mixing with the ambient fluid, the sediment concentrations of the turbidity current will vary not only per event, but per location and over time as well.

3 Results

3.1 Hydrodynamics of a turbidity current event

Two different stages of the turbidity current are identified based on the patterns described below. Firstly, an erosive, or waxing, stage during which net erosion occurs and the velocity of the current increases. This first stage dominates on the steeper slopes of the bathymetry. Secondly, a depositional, or waning, stage during which net deposition occurs and the velocity of the current decreases. The second stage dominates on the flatter parts and reversed slopes (Figure 3).

A current denser than the ambient water is observed to flow downslope during all modelled events. Several snapshots of the second event for a mixed composition model with zero and 100 m sill height are shown in Figures 4 and 5, respectively. The density and velocity magnitude at the front of the current both increase as the current flows down the slope (Figure 4A,B and Figure 5A,B). 'Instantaneous' erosion and deposition is defined here as the change in bed level with respect to five minutes earlier (i.e. the previous output time) [m/Δt]. Instantaneous erosion of the bed is observed as the current moves down the slope and increases simultaneously with velocity of the current (Figure 4A,B and Figure 5A,B). As the current moves towards less steep and even flat topography the velocity magnitude and density of the current decreases (Figure 4C,D and Figure 5C,D). A higher sill height leads to a greater decrease in velocity magnitude as the current reaches the opposite slope (compare Figure 4D and Figure 5D). Still some minor instantaneous erosion is observed at the front of the current, where velocity and density are highest. Sedimentation takes place upstream of this erosive front of the current. A distinction can thus be seen between the head of the current, which is erosive and slightly thicker than the rest of the current, and the body and tail region, from which sediment deposits. A velocity peak at the head of the current is observed to progradate to the water surface. The velocity vectors indicate that this phenomenon is part of the return flow, caused by the downstream boundary condition setting. As seen in Figures 4 and 5, the magnitude of this return flow can reach up to 2 m/s.

Spatial areas of net erosion and deposition can be distinguished after the event has passed (Figure 3). This cumulative erosion and sedimentation is defined as the change in bed level between the start and the end of the event, and therefore differs from the instantaneous erosion and sedimentation in terms of temporal scale. Net erosion is observed at the most landward slope situated between 0-8 km along the section. As shown in Figures 4 and 5, the velocity of the current increases as the head of the current moves over this interval. The increase in density during this same interval is attributed to the net sediment pick up from the bed. The net sediment pick up increases the negative buoyancy of the turbidity current, which causes it to accelerate. The transition from cumulative erosion to cumulative deposition occurs as the slope angle decreases and the current decelerates. This is attributed to a decrease of the negative buoyancy of the turbidity current. Although some instantaneous erosion was observed at the head of the current as it passed this interval (Figure 4C,D), the current as a whole was predominantly depositional. A second, smaller interval of cumulative erosion occurs at the slope towards the basin floor, 32-41 km along the section (Figure 3). This interval coincides with a steepening of the slope and a minor increase in velocity (compared to the velocity increase on the most landward slope), and is followed by net deposition where the slope flattens out into the ocean floor. However, this interval shows signs of a numerical instability, which is related to the change in slope around 40 km along the section. The numerical instabilities disappear for models with higher sill heights and are non-existent for the sand-rich composition model series. The numerical instability at the transition of slope to ocean floor has no further consequences for the rest of the model results, since the main point of interest lies with the ponded basin where no such instabilities occur.

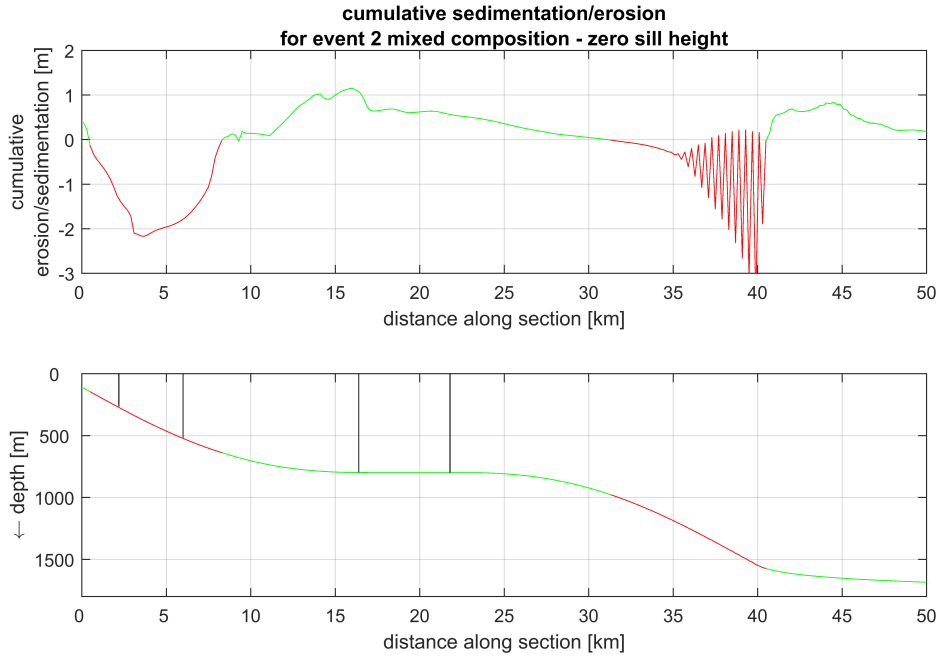

Figure 3: The top figure shows the cumulative erosion/sedimentation at the end of event 2 of the mixed composition - zero m sill height model series. The bottom figure shows the bathymetry along the first 50 km of section. Note how the areas with net erosion (red) coincide with the steeper slopes and the areas of net deposition (green) coincide with a flattening of the slope. The black lines in the upper figure indicate the locations where the snapshots in Figure 6 where taken.

These two different stages of the turbidity current are reflected in the sediment concentration profiles from different locations along the section (Figure 6, see Figure 3 for the locations of the profiles). These snapshots were taken approximately 600 m behind the front of the head for consistency. A clear step in the sediment concentration profile is observed at locations A and B (Figure 6A,B), that are both located on the first slope. A stepped sediment concentration profile as found on the slope is characteristic for erosional flows (Kneller and Buckee, 2000; Garcia, 1994). As the current reaches the flat slope, the sediment concentration profile becomes smoother and the concentrations decrease significantly (Figure 6D). A smooth concentration profile is characteristic for low-concentration, weakly depositional flows (Kneller and Buckee, 2000; Altinakar et al., 1996; Garcia, 1994). Furthermore, it is observed that the current height increases as the current moves down the slope. Location C is located within the interval of cumulative deposition, although the sediment concentration profile has the clear step characteristic for erosive flows. At this location the flow undergoes a transition from erosive to depositional, of which only the erosive character of the flow is captured by this early snapshot. The rest of the current's body will be predominantly depositional. The density structure of the flow thus reflects the erosional and depositional stages of the turbidity current as derived from the cumulative erosion and deposition patterns (Figure 3).

3.2 Amounts of erosion and ponded sedimentation

It is observed that the volume of sediment that is eroded on the first slope decreases with subsequent events (Figure 7). This observation is made irrespective of initial composition or initial sill height of the model. Event 1 of both the mixed and the sand-rich models are disregarded here, since the sediment concentration

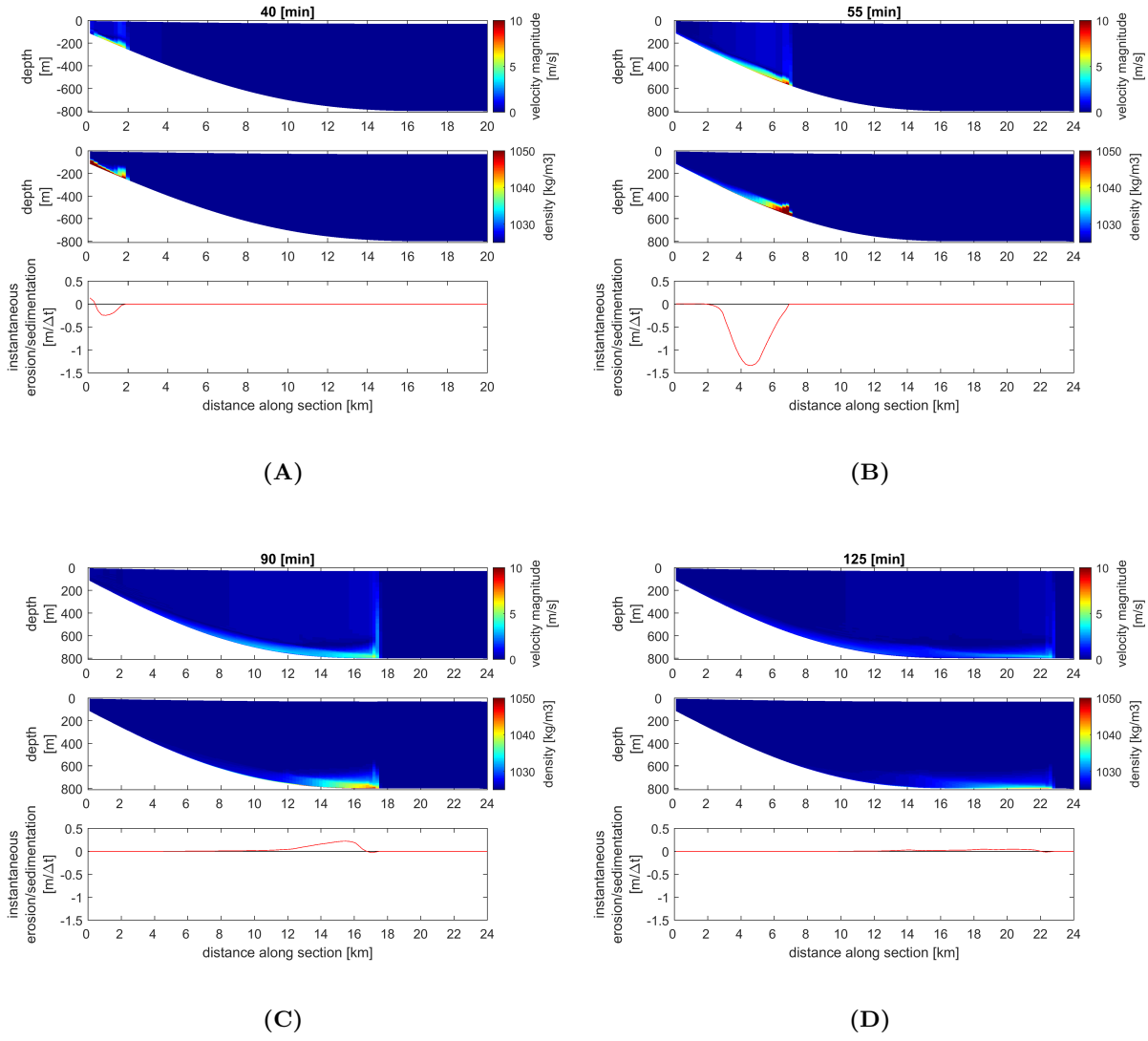

Figure 4: Plots of velocity magnitude, density and instantaneous erosion/sedimentation at four different time steps of event 2 of the mixed composition – zero m sill height series. See Figure 2 for the location of the cropped area shown here. A current with higher density than the ambient water is observed to flow downslope. Note that in the top two figures (A,B) the amount of instantaneous erosion increases as well as the size of the current. For the lower two figures (C,D) the velocity magnitude and density have decreased and mainly instantaneous deposition occurs. However, at the front of the current (where velocities and density are highest) instantaneous erosion occurs. Instantaneous erosion/sedimentation was derived by taking the difference in bed level with the previous model output time ($\Delta t = 5$ minutes). At the head of the current a velocity peak is observed to progradate to the water surface. The velocity vectors indicate that this phenomenon is part of the return flow, caused by the downstream boundary condition setting.

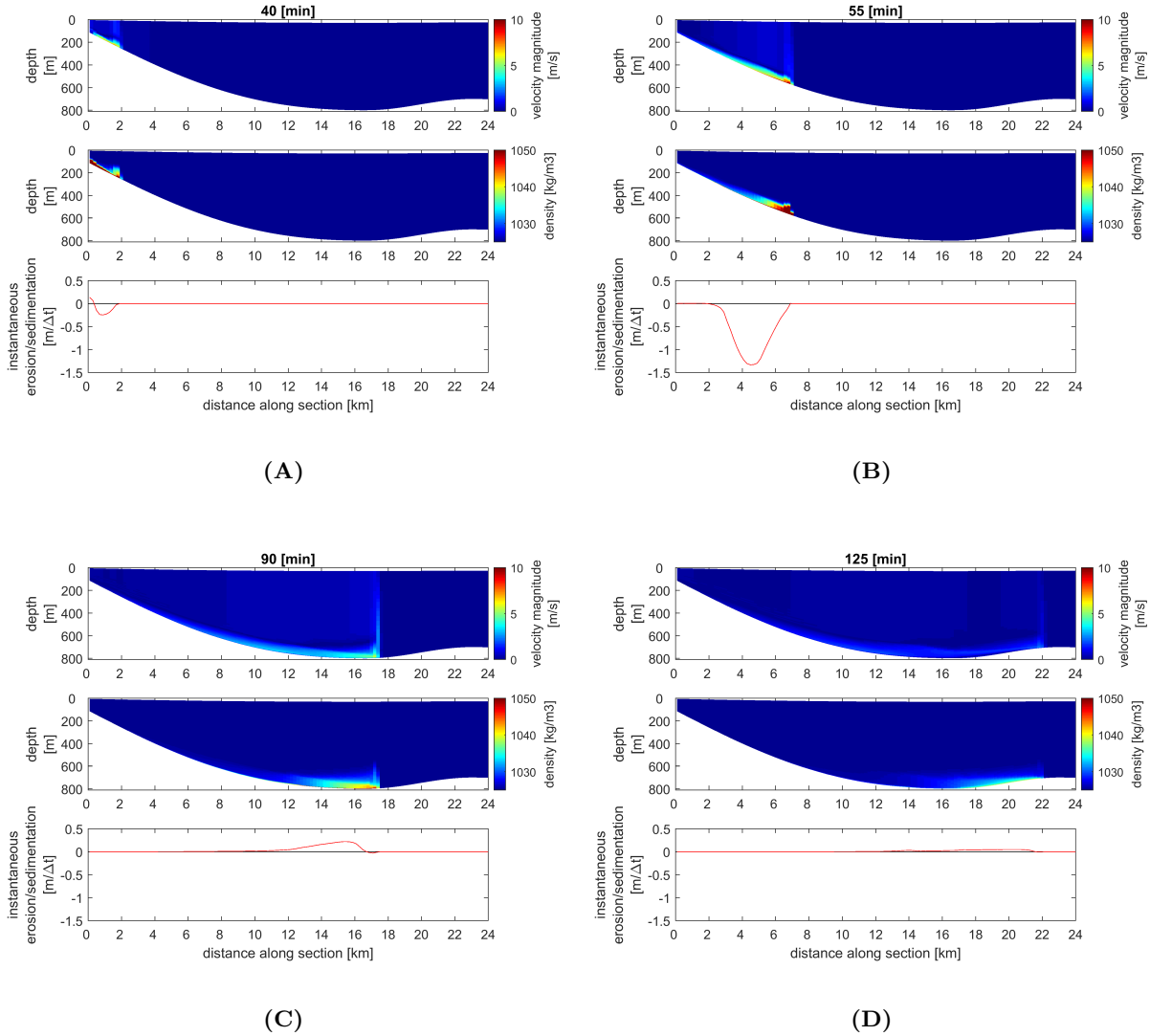

Figure 5: Plots of velocity magnitude, density and instantaneous erosion/sedimentation at four different time steps of event 2 of the mixed composition – 100 m sill height model series. See Figure 2 for the location of the cropped area shown here. Note that in the top two figures (A,B) the amount of instantaneous erosion increases as well as the size of the current, with no difference from Figure 4. However, the velocity magnitude of the current decreases more when the current reaches the opposite slope posed by the sill (D) than in case of zero sill height (Figure 4D).

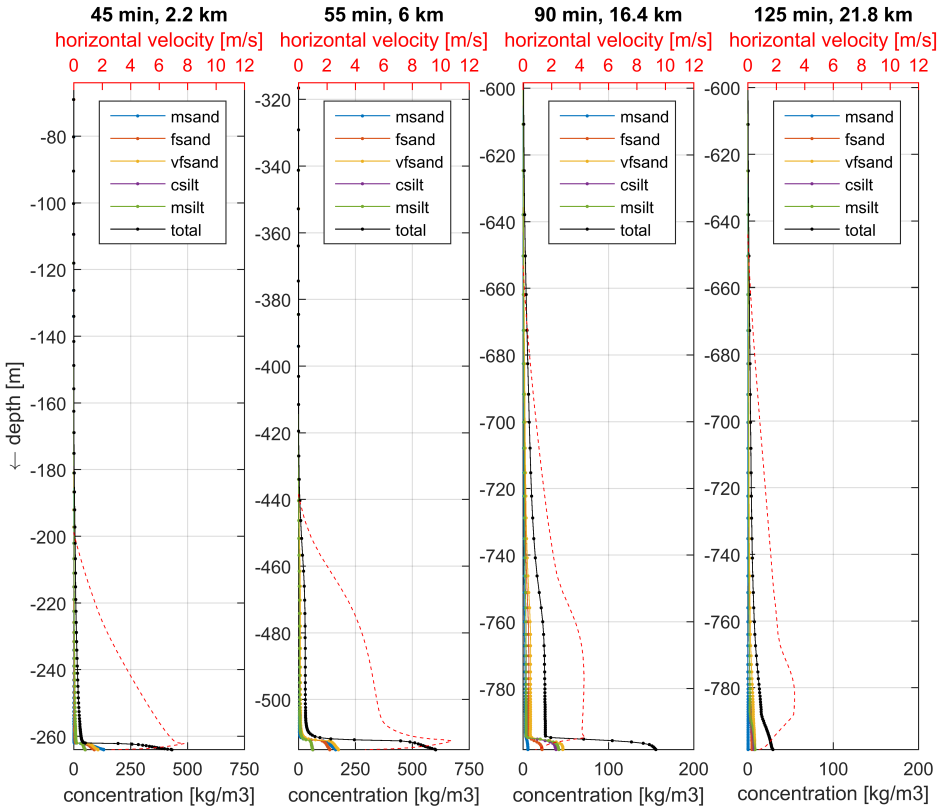

Figure 6: The sediment concentration and horizontal velocity profiles are shown at different locations for event 2 of the mixed composition – zero m sill height model series. The profiles are taken approximately 600 m landward of the head of the current. See Figure 3 for the locations of these profiles. The time steps coincide with the snapshots showed in Figure 4. The vertical spacing is equal for all profiles and that the vertical scale comprises the 200 m above bed level. Note that the horizontal scale for the sediment concentration changes for the different locations, due to the differences in sediment concentration. Furthermore it can be seen that the vertical resolution is smallest at the bottom and increases upward in the profile, due to the configuration of the grid (Section 2.2.1). See text for further explanation.

of their initial influx differs from the subsequent events 2-5 (Section 2.3.3).

Furthermore, it is noted that the initial sediment composition that is used, influences the amount of erosion that occurs. The mud-rich composition and sand-rich composition have the largest and smallest amounts of eroded sediment, respectively (Figure 7). In addition, the mud-rich and mixed composition models show larger amounts of eroded sediments for the lower sill height (0 m, 4 m and 20 m), whereas the sand-rich composition models do not.

The percentage of sediment that is 'trapped' or deposited within the ponded basin is calculated as the volume of sediment deposited between upstream boundary of the domain and the sill top (0 - 22.8 km), divided by the combined volume of sediment that is eroded on the most landward slope and dry bed volume equivalent of the sediment present in the initial influx. When plotted against the effective sill height, the data show a clear trend for each of the three initial compositions (Figure 8). In all three cases the percentage of sediment that is deposited within the ponded basin during each event, decreases together with the effective sill height of the model. However, the amount in which it decreases, differs per composition. For mud-rich and mixed composition models this relationship is similar, where 20 m sill height reduction leads to 5.3 % and 4.9 % respectively

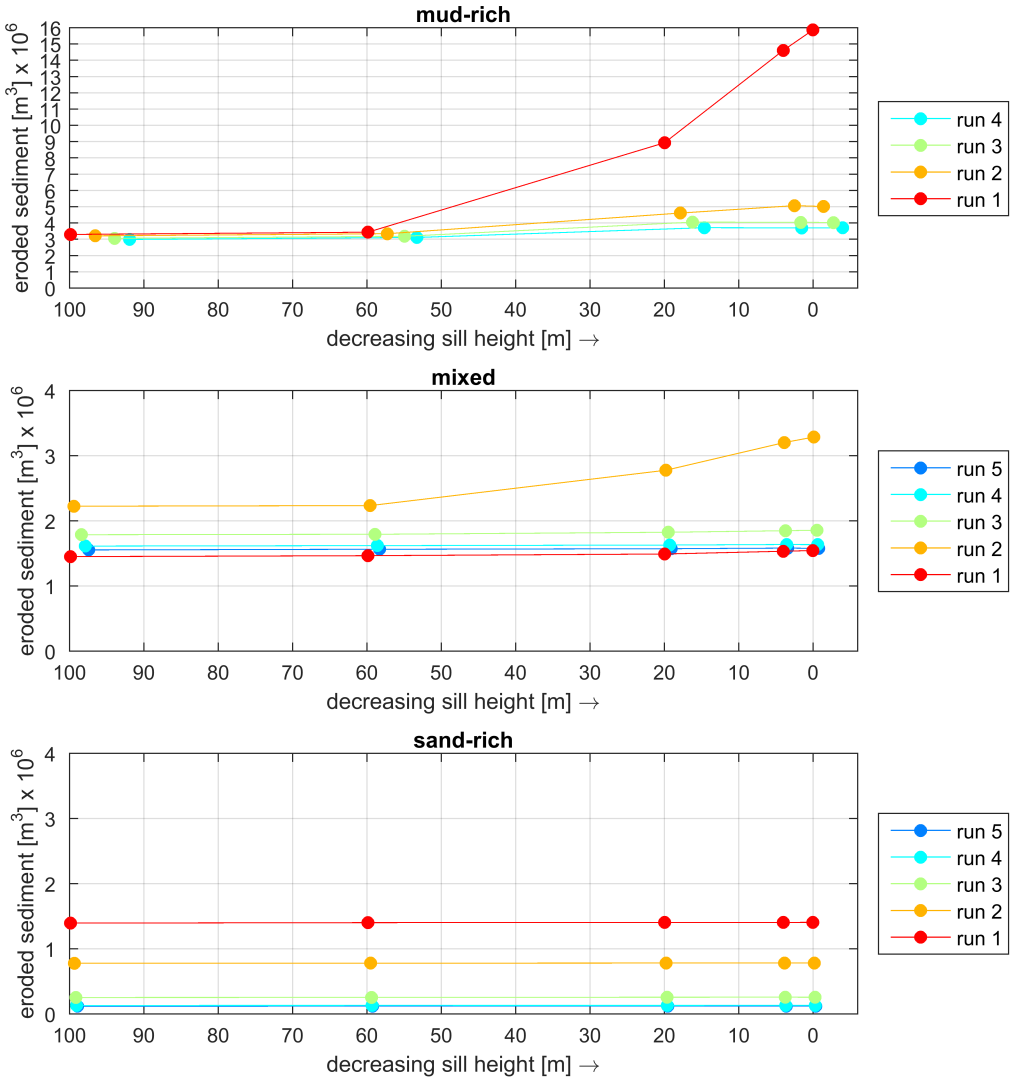

Figure 7: The amount of eroded sediment in millions m^3 versus the effective sill height in m is shown, for the three different compositions. Note that a decrease in volume of eroded sediment occurs for each subsequent run regardless of composition and initial sill height of the model.

less sediment captured in the ponded basin. For sand-rich composition models a 20 m sill height reduction leads to 2.8 % less sediment trapped.

With subsequent events within one model, the effective sill height of the model is reduced due to sediment deposition in the ponded basin. According to the relationship found above, subsequent events would have a lower percentage of sedimentation occurring in the ponded basin than the previous event, caused by increased overspill of sediment. Although this trend is observed in some models, it is not apparent in most models (Figure 8).

3.3 Synthetic wells

To get a detailed view of the stacking patterns in the sediments deposited by the turbidity currents, synthetic wells were made at multiple locations in the basin. These locations are located from 9.6 km to 22.8 km along the section (see Figure 2). At these locations, vertical bed profiles of the average grain size (D50) were made with a vertical resolution of 10 cm (Figure 9).

3.3.1 Stacking patterns

Individual turbidites are recognized by an increase in D50 at the base and a more gradual decrease to lower D50 at the top. No intervals of hemipelagic mud are present between the turbidites, since background sedimentation was excluded from the model. These beds are readily distinguished in the mixed and mud-rich composition models (e.g. Figure 9A,B,D,E), but less clearly distinguished in the sand-rich composition models (e.g. Figure 9C,F). A 10 cm vertical resolution is large with respect to the expected bed thicknesses of <30 cm for the sand-rich composition models. It is hypothesized here that the vertical resolution is unable to capture the coarsening upward pattern distinctive for the base of individual beds, in the sand-rich composition models. Instead of five individual turbidites, only an overall fining upward trend is observed. For the mud-rich composition models a second coarsening up and fining up pattern can be distinguished at the top of each bed at locations 16.6 km to 19.6 km (Figure 9A,B). This is attributed to a minor increase in flow strength of the tail of the current. Furthermore, the thickness of the individual turbidites decreases with decreasing sill height. This effect is less pronounced at the sill top (location 22.8 km) (Figure 9).

Based on these vertical profiles the average D50 per bed is determined for the mixed and mud-rich composition models. An overall decrease in average grain size along the section of the ponded basin is observed for all deposited beds.

In general, the formed set of beds in mixed and mud-rich composition model series is fining upward. In this trend event 1 for the mixed composition models is neglected since the initial influx conditions differ from the subsequent events (Section 2.3.3).

3.3.2 Relation D50 and non-cohesive volume fraction vs. amount of confinement

The mean grain size and the volume ratio between sand and mud are important characteristics for the reservoir potential of turbidites. The D50 and non-cohesive volume fraction of the turbidites deposited by each event, are plotted against the original sill height of the model to assess the evolution of these characteristics with decreasing sill height. The results at four locations are shown in Figures 10-11 and 12-13 for the mixed and mud-rich compositions respectively. The model series with sand-rich composition are not included in this analysis because individual turbidites could not be clearly distinguished from the synthetic well data of these model series. Location 13.4 km is on the first slope, 16.6 km is the basin centre, 19.6 km is on the opposite slope towards the sill top and 22.8 km is located on the sill top (Figure 2).

Mixed composition In the model series with mixed composition, the D50 of each bed is seen to increase when the sill height of the

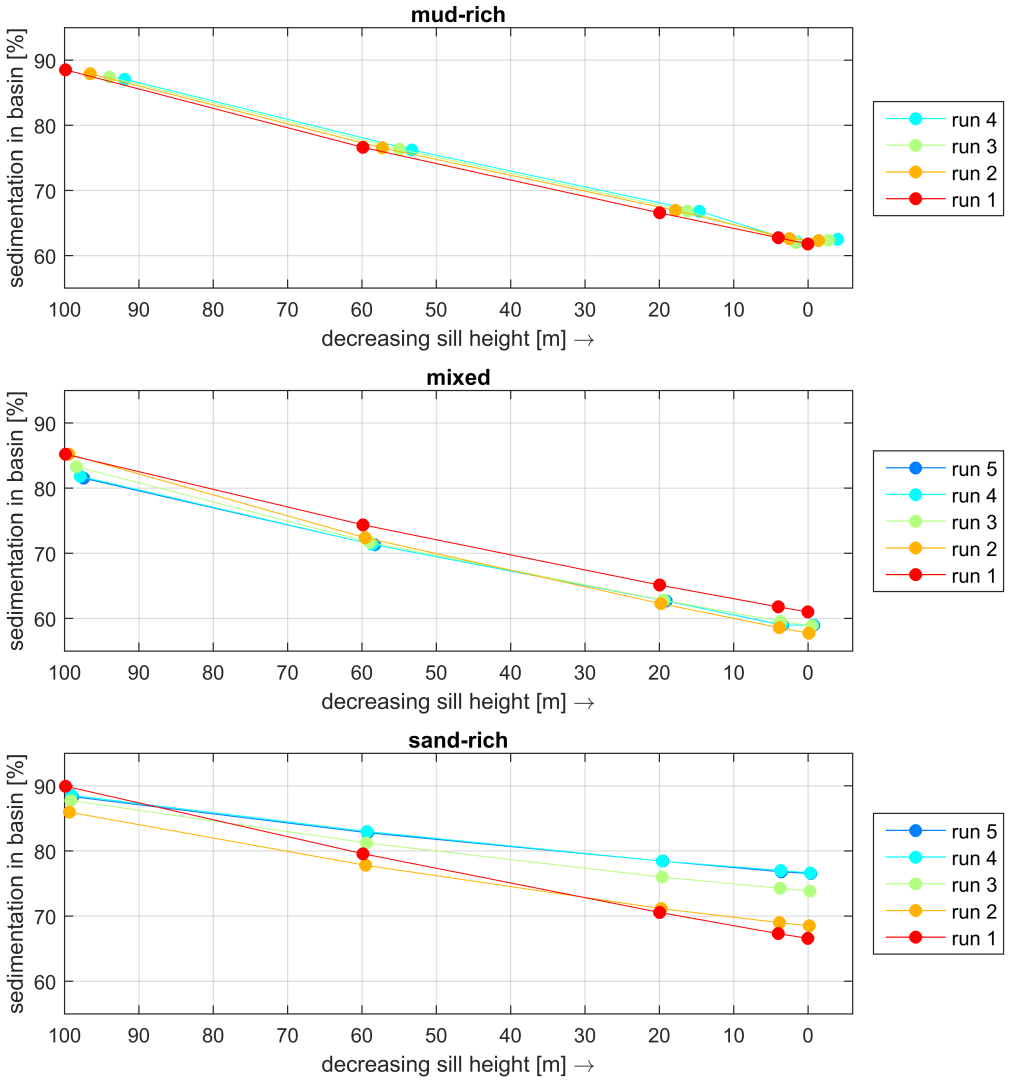

Figure 8: The percentage of sediment that is trapped within the ponded basin versus the effective sill height of the run is shown, for the three different compositions. With lower sill height, the percentage of sedimentation that occurs within the ponded basin decreases as seen between the model series with different sill heights.

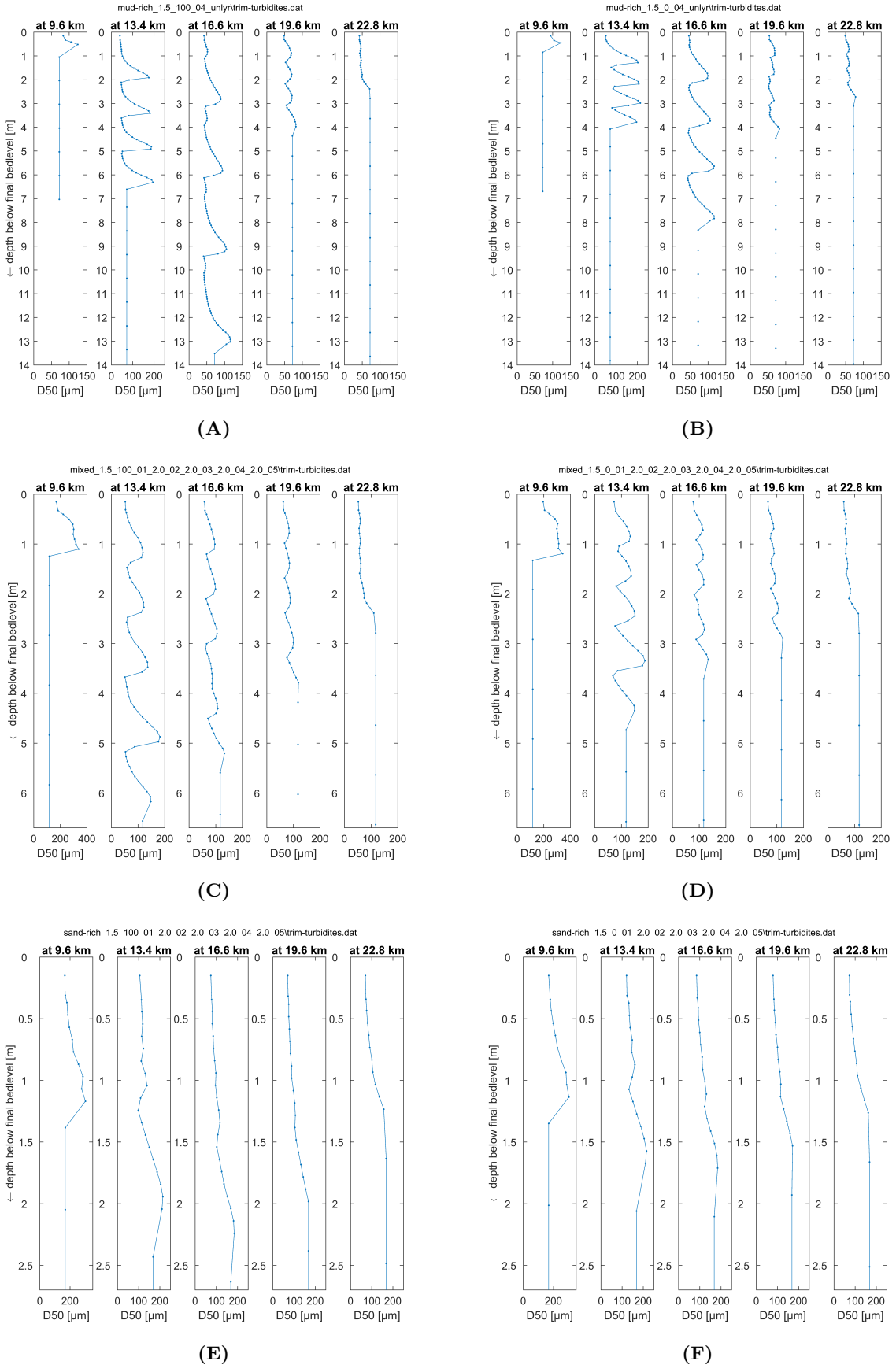

Figure 9: See following page.

Figure 9: The vertical D50 profiles are shown at multiple locations in the ponded basin for zero sill height model series with mud-rich composition (A), mixed composition (B) and sand-rich composition (C), and for 100 m sill height model series with mud-rich composition (D), mixed composition (E) and sand-rich composition (F). Note the differences in vertical scale between the different compositions due to differences in deposit thickness and the differences in horizontal scale due to large differences in grain size. In general fining upward stacking patterns are observed irrespective of composition and sill height of the model. The total thickness of the deposit decreases with lower sill heights. Furthermore it is noted that individual beds are not readily distinguished in the sand-rich composition models. See text for further explanation.

model decreases, for locations 13.4 km (first slope) and 16.6 km (basin centre). Furthermore, this effect is stronger at location 13.4 km (i.e. slope of graph is steeper) than in the basin centre (Figure 10A,B). At the sill top (location 22.8 km) two different trends can be distinguished. From 100 to 20 m sill height the D50 the trend is concurrent with the trend found at locations 13.4 km and 16.6 km. From zero to 20 m sill height, however, D50 stays constant with decreasing sill height. At the opposite slope between the basin centre and sill top (19.6 km) these trends are reversed (Figure 10C). Here D50 stays relatively constant between 100 m and 20 m sill height and between 20 m and zero m sill height the D50 increases with decreasing sill height.

In general, the same trends are observed when looking at the non-cohesive volume fractions. However, at location 19.6 km the non-cohesive volume fraction decreases slightly between 100 m and 20 m sill height (Figure 11C), indicating that the smaller, cohesive sediment fraction increases although this is not apparent as a decrease in average grain size (Figure 10C). The same applies to location 22.8 km, where the non-cohesive volume fraction decreases slightly between 20 m and zero m sill height (Figure 11D), although the D50 remains constant (Figure 10D).

Mud-rich composition For the models with mud-rich composition the average D50 of each bed increases when the sill height of the model decreases at locations 13.4 km (first slope) and 16.6 km (basin centre) (Figure 12A,B). This corresponds with the trends for the mixed composition models at these locations (Figure 10A,B). Although the D50 of the initial mud-rich composition sediment is lower than the D50 of the initial mixed composition sediment, the D50 of the deposited beds at location 13.4 km (first slope) is similar or even larger than the D50 of the mixed composition model beds at that locality.

At the sill top (location 22.8 km, figure 12D) two trends can be distinguished. From 100 m to 20 m sill height D50 increases with decreasing sill height. This is followed by a constant D50 from 20 m to zero m sill height. The non-cohesive volume fraction at this locality (Figure 13D) increases from 100 m to 20 m sill height and decreases slightly between 20 m and zero m sill height. At the opposite slope (19.6 km) both D50 and non-cohesive volume fraction increase slightly from 100 m to 60 m sill height, and both show a decrease as sill height decreases from 60 m to zero m (Figure 12C and 13C).

4 Discussion

4.1 Inherent sensitivity to autogenic changes in substrate erodibility

4.1.1 Presence of more cohesive material leads to larger amounts of erosion

The use of a different initial sediment composition results in different amounts of erosion during the waxing stage of the turbidity current. A mud-rich composition produces larger amounts of erosion than mixed and sand-rich compositions (Figure 7). These differences in substrate erodibility are related to grain size and sediment composition. A higher shear stress is

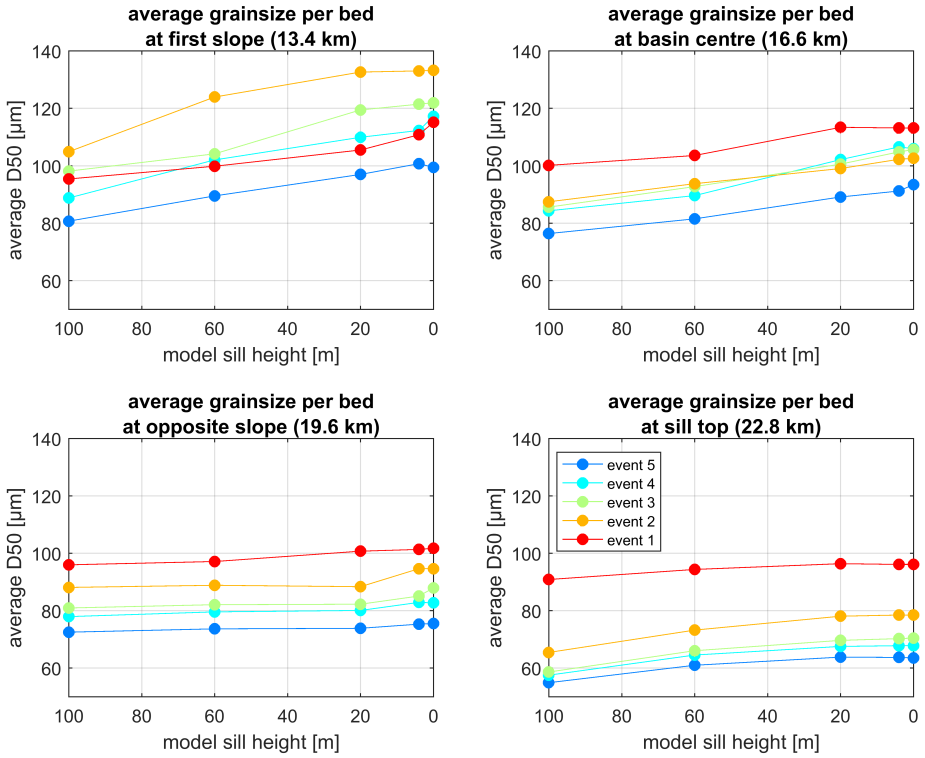

Figure 10: The average mean grain size (D50) of the beds deposited during one event is shown as a function of the model sill height for the mixed composition model series, at four different locations. A is located on the first slope (13.4 km), B in the basin centre (16.6 km), C on the opposite slope towards the sill top (19.6 km) and D at the sill top (22.8 km). The data of event 1 is dotted, since the concentration of the initial influx differed from that of events 2 to 5. See text for further description of the observed trends.

needed to erode larger grains. At the onset of the current, this effect will favour (more) erosion in the finer-grained mud-rich composition models than in the mixed and sand-rich composition models.

Based on the Shields curve (Figure 14A) it is expected that cohesive forces between particles of the cohesive sediment classes would increase the critical shear stress needed to erode the sediment. The presence of cohesive particles in a heterogeneous sediment mixture, such as applied in this study, would decrease the substrate erodibility (Mitchener and Torfs, 1996; Panagiotopoulos et al., 1997). However, Postma (1967) described a positive correlation between consolidation and critical shear stress. The effect of cohesion on the erodibility of the sediment mixture is only observed if the mixture is consolidated enough (Figure 14B). Effects of consolidation and compaction of the deposited sediment are not taken into account by the model presented in this study. Including the effects of consolidation and compaction on cohesive behaviour and the substrate erodibility would therefore be considered an improvement of the current model. However, the erodibility of cohesive sediment is influenced by a wide range of physical, geochemical and biological properties (Grabowski et al., 2011, and references therein). With the current understanding of these properties and their interaction, the development of a unifying equation to predict erodibility remains difficult (Grabowski et al., 2011).

The turbidity currents generated in the mud-rich composition models remain erosive farther

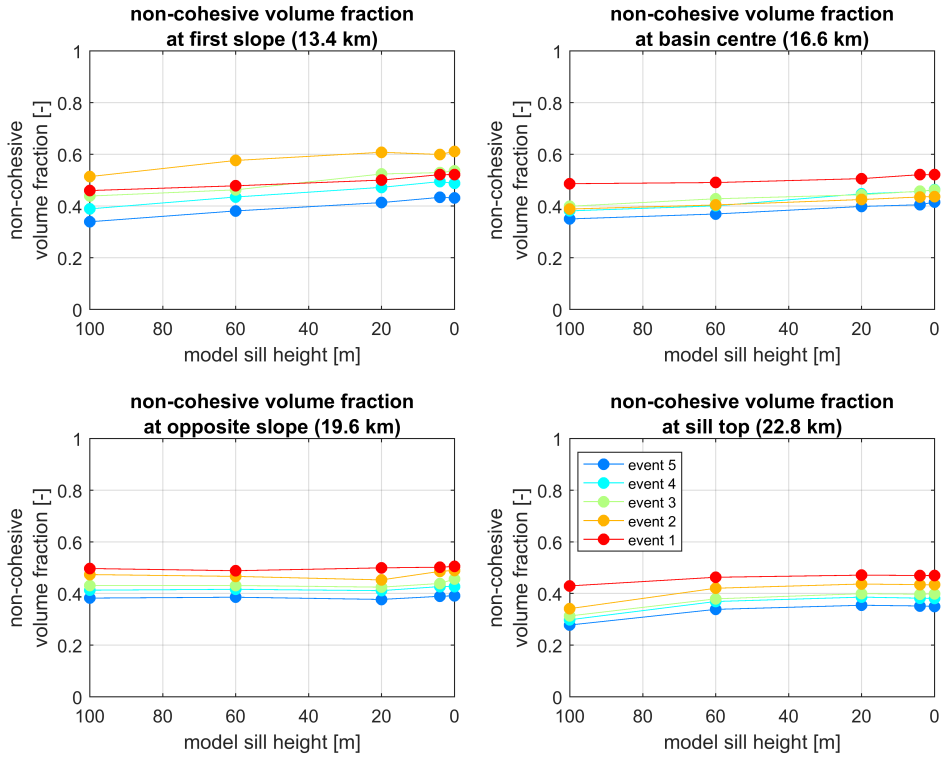

Figure 11: The non-cohesive volume fraction of the deposited beds is shown as a function of the model sill height for the mixed composition model series, at four different locations. Note the accordance with the trends in Figure 10A,B and the difference in trends between C,D and Figure 10C,D.

down the slope than mixed and sand-rich composition currents (Figure 15). This is related to their flow efficiency, which is defined as the ability of the flow to carry sand in a basinward direction (Mutti, 1992). This ability is controlled by the grain size composition of the suspended sediment load and the flow volume. Low efficient flows have a relatively small volume and/or are generally loaded mainly with coarse grained sediment (Mutti, 1992), while flows with high efficiency have a relatively large volume and/or contain high amounts of fine-grained sediments (Al Ja'Aidi et al., 2004). In the results of this study, the mud-rich composition models generate relatively more efficient flows that remain net erosive for a longer distance and become net depositional later than the mixed and sand-rich composition models respectively (Figure 15). The increase in flow efficiency for mud-rich composition models is attributed to the erosion and entrainment of mainly fine-grained sediment. Therefore, the currents generated by the mud-rich composition models do not only have the highest efficiency compared to the other initial compositions, the currents can erode the substrate over a longer distance and hence have a larger total amount of erosion.

The results of this study indicate that the modelled flow dynamics of the turbidity current and the amount of sediment picked up by the current are influenced by the composition and hence erodibility of the substrate. It was stated by Traer et al. (2012) that flow dynamics in any numerical model of turbidity currents are highly sensitive to subtle changes in the entrainment parameters, due to presence of empirical relationships in the formulations used by such a model. In addition, flow dynamics are shown to be highly sensitive to autogenic changes in the substrate erodibility, when parameters describing erosion and sedimentation

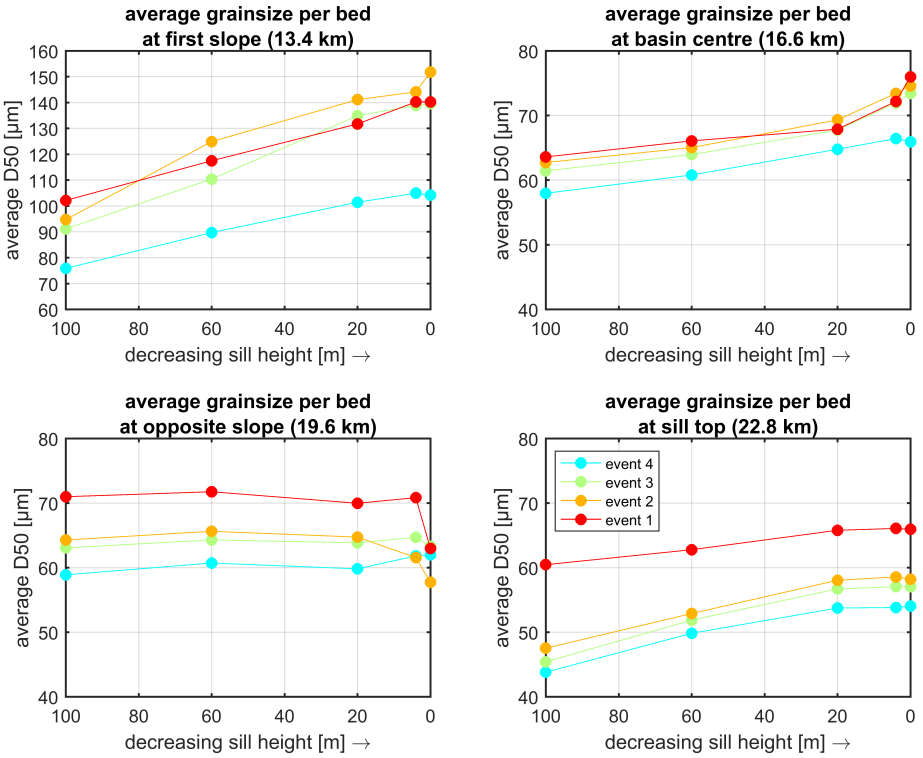

Figure 12: The average mean grain size (D50) of the beds deposited during one event is shown as a function of the model sill height for the mud-rich composition model series, at four different locations. A is located on the first slope (13.4 km), B in the basin centre (16.6 km), C on the opposite slope towards the sill top (19.6 km) and D at the sill top (22.8 km). See text for further description of the observed trends.

are kept equal in all simulations. Therefore, this observation supports the idea that this sensitivity is inherent to turbidity currents themselves, and not solely a flaw from the formulations used in numerical models.

4.1.2 Autogenic coarsening of the slope substrate

A decrease in total amount of eroded sediment was observed between subsequent events within one model, irrespective of initial composition and sill height used (Figure 7). This is attributed to the autogenic coarsening of the substrate. With each subsequent event the sediment on the slope that remains after the previous event becomes coarser (Figure 16). Based on their laboratory experiments, Sequeiros et al. (2009) posed the idea that the presence of fine, easily entrainable material at the top of the previous deposit promoted self-acceleration of the subsequent current. Conversely, the coarser substrate remaining on the slope after previous events in this study leads to less erosion, which suggest that the lack of fine, easily entrainable material 'hinders' or at least leads to less self-acceleration. Thus, the differences in erodibility of the substrate that lead to the different amounts of erosion between the different composition models also have a noticeable effect between deposits of subsequent events. This supports the idea of inherent sensitivity of turbidity currents to changes in erodibility of the substrate.

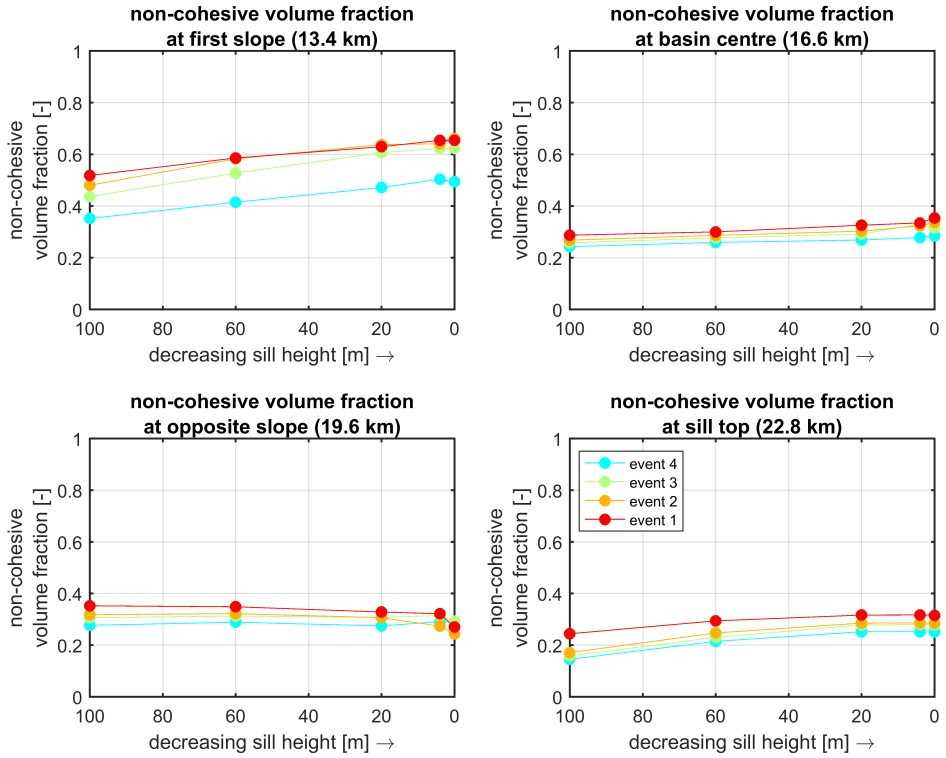

Figure 13: The non-cohesive volume fraction of the deposited beds is shown as a function of the model sill height for the mixed composition model series, at four different locations. Note the accordance with the trends in Figure 12A,B and the difference in trends between C,D and Figure 12C,D.

4.1.3 Particle-particle interactions

The near-bed sediment concentrations can reach high values as the turbidity current moves downslope (Figure 6). A sediment concentration of approximately 500 kg/m^3 corresponds to a volumetric sediment concentration of approximately 19 %. For volumetric sediment concentrations larger than circa 10 % particle-particle interactions become important and hindered settling starts to occur (Bagnold, 1954). The Delft3D-FLOW module follows Richardson and Zaki (1954) to account for the effect of hindered settling. However, whether this approach is sufficiently suitable for turbidity currents with near-bed volumetric sediment concentrations of nearly 20 %, is debatable.

Meiburg et al. (2015) mark the understanding of the dynamics in the high concentration near-bed region as an ongoing challenge for computational modelling of gravity and turbidity currents. The implementation of improved and validated formulations regarding the dynamics in the near-bed region, would attribute to the confidence of the model presented in this study.

4.2 Allogenic control on recurrence interval of self-accelerating turbidity currents

Following the section above, it is proposed that subsequent flows become less and less efficient due to this decrease in available fine sediments, until the point where they no longer self-accelerate and sediment is only deposited on the slope by a waning flow. This key role that the availability of fine, easily entrainable bed material plays in determining whether a turbidity current will self-accelerate or not has been previously noted by Sequeiros et al. (2009).

Depending on the material present on the

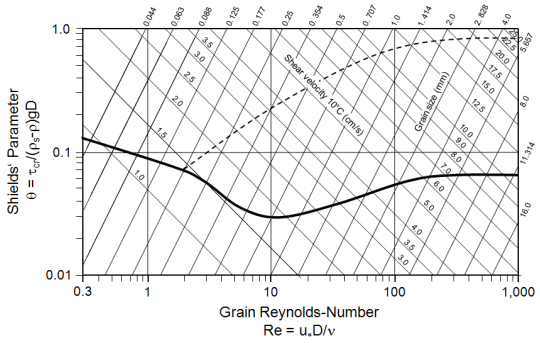

(A)

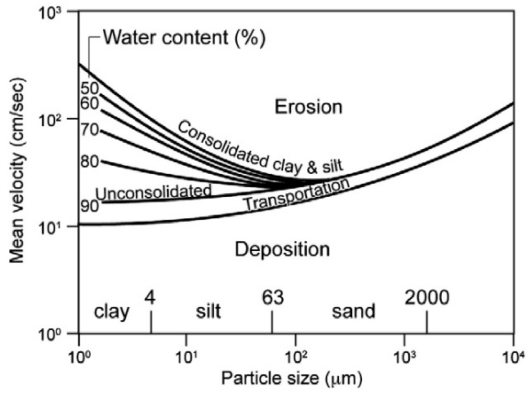

(B)

Figure 14: Shows the Shields (a) and Postma (b) diagrams that show the thresholds for erosion and deposition according to average particle size. After Van Rijn et al. (1993) and Grabowski et al. (2011), respectively.

bed, a turbidity current can become either waning, where all sediment is deposited on the slope, or self-accelerating, where sediment is transported to and deposited in the basin. Multiple ways in which a transition from waning flow to self-accelerating turbidity current might reoccur are put forward here.

1) The deposition of fine material by background sedimentation might counteract the coarsening of the substrate with each event, such that the following current will self-accelerate again. 2) A change in type of sediment supply towards the continental shelf could also counteract the coarsening of the substrate with each event. 3) The occurrence of a larger initial influx (e.g. representing a larger slope failure or river discharge) produces a stronger current that has enough potential to pick up the coarser sediment left on the slope, and flush the canyon. However, this would still require the replenishment of fine material afterward, or the initial influx has to keep increasing.

Changes in background sedimentation rate, type of sediment supply to the continental shelf and size of the initial influx are all related to allogenic processes such as eustasy, climate and tectonics. Either a constant background sedimentation rate could suffice to counteract the coarsening of the substrate, or a change in allogenic process is needed to facilitate the transition from waning current to a self-accelerating current. Therefore, these allogenic processes and constant background sedimentation are put forward as controls on the recurrence interval of self-accelerating turbidity currents. Only self-accelerating turbidity currents deposit sediment in the ponded basin. Therefore, these processes in fact control the recurrence interval of turbidity currents in ponded basins and hence have a strong control of the resulting basin stratigraphy. Further research is recommended to constrain these controls.

4.3 Overprinting of fill-and-spill signature by subsequent events

4.3.1 Amount of overspill

The percentage of sedimentation that occurred within the ponded basin was less than 100 % of the sediment supplied and eroded from the substrate, during all events. Hence, these flows are classified as partially ponded or partially confined (Brunt et al., 2004). The primary relation found between model series with different sill heights is that with decreasing sill height the percentage of sediment trapped in the ponded basin decreases. This relationship is attributed to the fact that a larger part of the flow is able to spill over if the sill height is reduced and hence less sediment is deposited within the ponded basin itself. The results of the simulated turbidity current events in this study are consistent with the fill-and-spill model and with the 'flow stripping' phase of the depositional model proposed by Sinclair and Tomasso

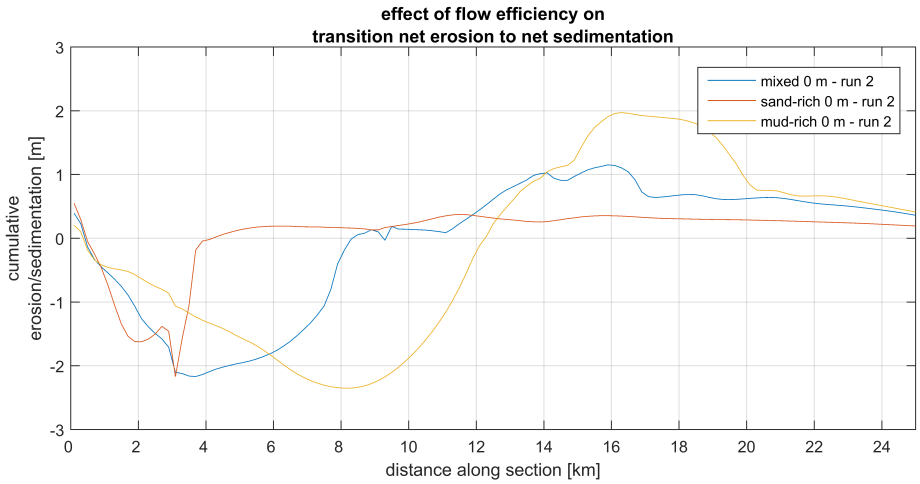

Figure 15: The cumulative erosion/sedimentation patterns are shown for event 2 of the three different compositions – zero sill height model series. Note that the transition from net erosion to net sedimentation occurs nearest for the sand-rich composition run and farthest along the section for the mud-rich run. See text for further discussion.

(2002) for the progressive infill of confined turbidite basins.

This primary relation is not always observed between subsequent events where the model sill height is progressively reduced with each event due to sediment deposition in the ponded basin (Figure 8). This deviation of the trend demonstrates the interplay of three different processes and effects between subsequent events. Firstly, the coarsening of the eroded substrate with each subsequent event leads to a smaller amount of eroded sediment. This results in a decrease in flow strength which makes the flow effectively more confined by the sill. Secondly, reduction of the sill height, which depends on the sediment volume deposited by the previous current and the geometry of the ponded basin, makes the flow effectively less confined by the sill. Thirdly, the flow efficiency of the current influences the geometry of the ponded basin. For low efficiencies the slope may be extended further into the basin, as currents with low efficiencies tend to deposit their sediment load in the proximal zone (Amy et al., 2007). In contrast, more efficient currents carry their sediment load further into the basin and mainly cause aggradation on the basin floor. These differences in resulting slope morphology will alter the hydrodynamics and, effectively, the strength of subsequent turbidity currents.

These processes and effects described in the previous paragraph signify the complex interrelation of multiple processes that cause the deposits of subsequent events to deviate from the primary relationship between sill height and the percentage of sediment 'trapped' in the ponded basin.

4.3.2 Fining upward stacking pattern

With a fill-and-spill depositional model, not only is it expected that more material spills over the ponded basin with decreasing sill height, but due to vertical grain size stratification of turbidity currents (Peakall et al., 2000) the deposits of subsequent flows will become increasingly sand-rich (Brunt et al., 2004). A coarsening upward stacking pattern is thus expected in case subsequent flows have identical properties. However, with subsequent events a fining upward stacking pattern is found (Figure 9). This is again attributed to the autogenic effect of erodibility of the substrate, which leads to a decrease in flow strength of subsequent events. This causes the expected coarsening up stacking pattern, which is thought to be characteristic for a fill-and-spill setting, to become effectively overprinted by a fining up stacking

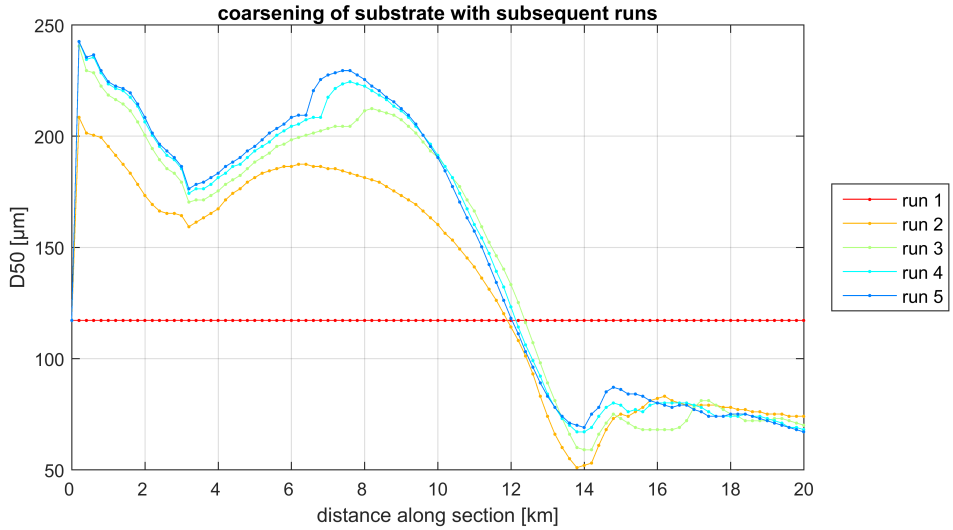

Figure 16: The coarsening of the substrate present at the proximal part of the slope (1-10 km) is shown with subsequent events of the mixed composition – zero m sill height model series. The D50 shown here corresponds to the average grain size of the 30 cm thick transport layer at the bed surface.

pattern.

4.4 Linking two temporal and spatial scales

Two contradictory trends in grain size with decreasing sill height are seen, which can be related to different temporal and spatial scales. At the temporal and spatial scale of subsequent turbidites a fining upward stacking pattern is found in the deposits. The fining upward stacking pattern is attributed to autogenic coarsening of the slope substrate with each subsequent event. The erodibility of the substrate therefore proves to be the main autogenic control that affects the depositional patterns within the basin at this scale.

The difference in sill height between the consecutive model series ranges from 4 to 20 m. A sediment package of this range is better represented on the scale of turbidite lobes or lobe complexes, rather than on the scale of individual turbidites. Therefore, the model series with different sill heights is believed to represent a larger temporal and spatial scale of lobes or lobe complexes. At this scale the average grain size of the deposits is seen to increase as sill height decreases and a larger percentage of sediment is able to spill over. The effects of flow stripping in a fill-and-spill basin are thus recognizable in the depositional characteristics of the turbidites at this scale.

The contradiction between the two temporal and spatial scales illustrates that at a larger scale, the autogenic effect of coarsening of the substrate on the slope is counteracted by constant background sedimentation or changes in allogenic processes such as background sedimentation rate, sediment type and size of initial influx. Without these external controls no stacking of multiple turbidite lobes would occur in the ponded basin.

It is noted, that the 2DV approach used in this study, is unable to capture depositional patterns in 3D. Therefore, the effects of compensational stacking and channel avulsion could not be assessed. Both compensational stacking and channel avulsion have been identified as autogenic processes influencing the 3D stacking pattern in turbidite fan complexes (Prélat et al., 2009). However, changes in autogenic coarsening of the substrate is the main process that affects the depositional patterns of subsequent turbidites within a 2DV ponded basin. The importance of the effect of autogenic changes in substrate erodibility should also be assessed in 3D settings.

4.5 Conceptual model for grains size trend evolution in ponded basins

Figure 17 shows a conceptual model which summarizes and illustrates how the grain size trends observed in this study depend on the sill height and the location in the ponded basin.

When comparing the grain size trends between models with different sill height, at the proximal and basin centre locations (13.4 km and 16.6 km), a coarsening of the average bed grain size is observed, with decreasing sill height (Figure 10A,C and 12A,C). Combined with the fact that more overspill occurs with lower sill heights, this is consistent with the fill-and-spill concept where reduction in sill height would lead to more fine material spilling over and a coarser deposit being left in the ponded basin.

However, this straightforward relationship is altered at the top of the sill and on the opposite slope (location 22.8 km and 19.6 km respectively). At the top of the sill a constant D50 and a slight decrease in the non-cohesive volume fraction from 20 to 0 m sill height infer that the coarsening upward pattern related to more overspill of fine sediment, stops when the sill height becomes less than 20 m. For lower sill heights the proportion between fine and coarse sediment does no longer change with decreasing sill height. Both fine and coarse sediment are bypassed in the same proportion. This effect causes the D50 and non-cohesive volume fraction to remain constant for these low sill heights. This is effectively the transition from the flow stripping stage to the flow bypass stage as described by Sinclair and Tomasso (2002).

The exact sill height at which this transition occurs is here related to the flow runup height with respect to the sill height. The runup height is defined by Straub et al. (2008) as a balance between kinetic energy of a current and the potential energy needed to overcome a certain height. This runup height represents an upper limit as the effects of friction on the energy budget are neglected (Straub et al., 2008). Based on the formula presented by Straub et al. (2008) the average runup height for the mixed and mud-rich composition models is 27 m and 13 m respectively. These runup heights agree quite well with the 20 m sill height where a shift in grain size and cohesive volume fraction trend is observed, considering the resolution of the five different sill heights used in this study.

On the opposite slope, between the basin centre and on the sill top, the non-cohesive volume fraction decreases and the D50 stays relatively constant when the sill height is reduced towards the runup height of the current. This is attributed to the fact that with decreasing sill height an increasing amount of non-cohesive (coarser) material is partially bypassed farther up or over the sill. This effect of increased bypass of coarser material counteracts the coarsening upward fill-and-spill signature of more overspilling of fine sediment, found at the more proximal locations (figure 17).

If the sill height becomes lower than the runup height of the current, this signature is no longer counteracted by this bypass-effect for the mixed composition models (Figure 17). For the mud rich composition models the non-cohesive volume fraction continues to decrease for low sill heights (<20 m) instead of increase as for the mixed composition models. This difference between the trend for mixed and mud-rich composition models at this locality (19.6 km) might be related to differences in the grain size stratification or flow efficiency between the two different compositions.

5 Conclusions

Differences in amount of erosion and hence the size of the resulting surge-type turbidity current between models with mud-rich, mixed and sand-rich compositions are explained in terms of changes in substrate erodibility. The presence of more cohesive material in the initial sediment composition leads to larger amounts of erosion. This is related both to preferential erosion of finer sediment and the higher efficiency of mud-rich flows. The substrate that remains on the slope becomes coarser with subsequent events. This autogenic coarsening of the substrate leads to less erosion with subse-

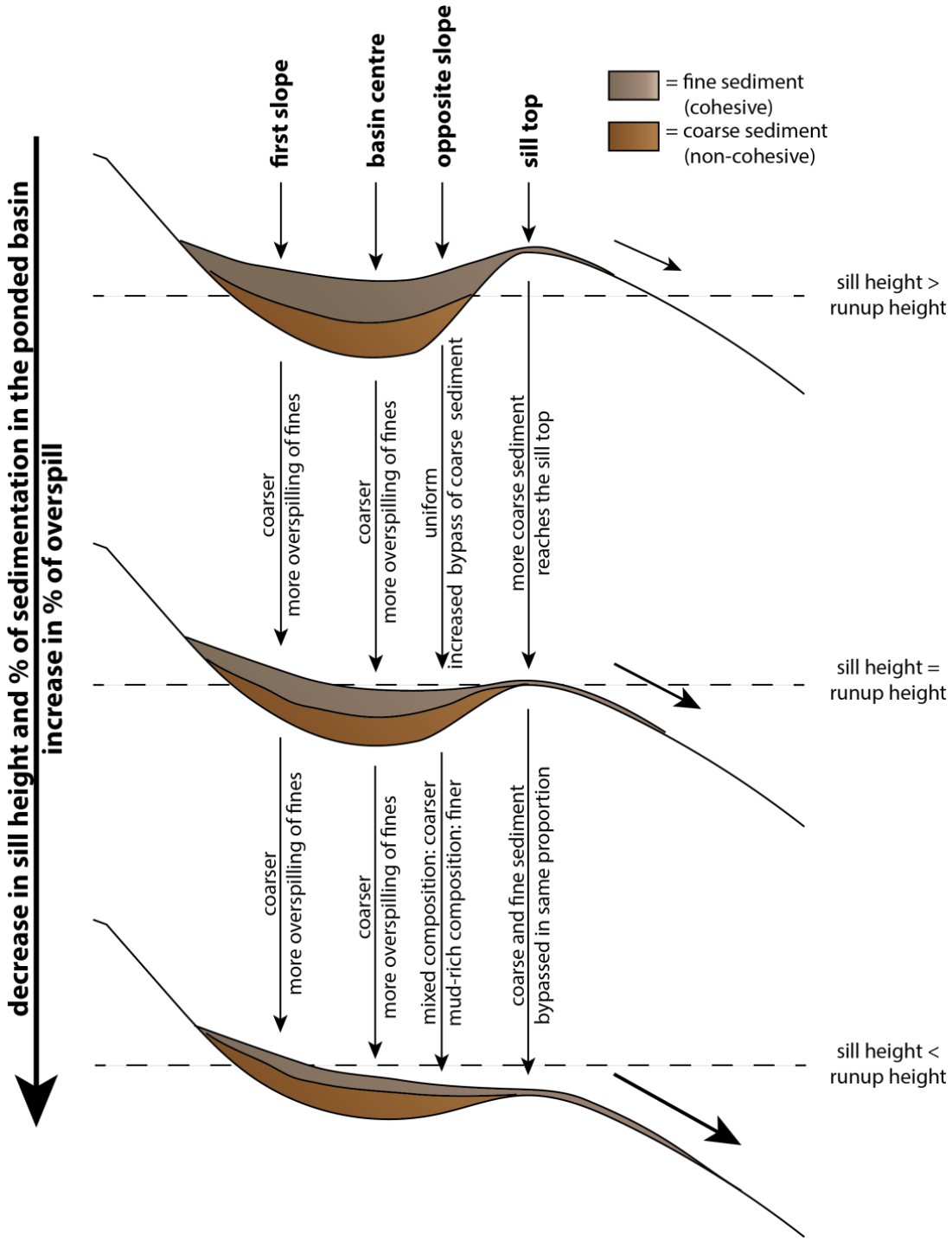

Figure 17: A schematic model is proposed to explain the differences in grain size trends with decreasing sill height for different locations in the ponded basin. Excess deposition in the basin with respect to the sill always causes a decrease in sill height over time. Stage A shows the trends if the sill height is larger than the runup height of the turbidity currents. Stage B shows the trends at the different locations if the sill height is smaller than the runup height of the current. Note that the trend does not change between the two stages for the two proximal locations (first slope and basin centre), whereas the change from stage A to B results in different trends for the more distal locations (opposite slope and sill top). See text for further explanation.

quent events, consequently leading to smaller flows. This study supports the idea of Traer et al. (2012) that turbidity currents have an inherent sensitivity to changes in erodibility of the substrate and that this is not a remnant from the formulations used in numerical models.

It is proposed that subsequent flows become less and less efficient due to the autogenic coarsening of the substrate, until the point where they no longer self-accelerate. A constant background sedimentation or change in allogenic process is needed to facilitate the transition from waning current to a self-accelerating current. Therefore, constant background sedimentation or changes in allogenic processes are put forward as controls on the recurrence interval of turbidity currents in ponded basins.

The primary relation found between model series with different sill heights is consistent with the fill-and-spill concept and with the 'flow stripping' phase of the depositional model proposed by Sinclair and Tomasso (2002). However, with subsequent events of a model series this primary relation is generally not met and depends on the interplay of the following effects: flow strength, reduction of sill height, flow efficiency and geometry of the ponded basin. For subsequent events a fining upward stacking pattern is found, which is attributed to the autogenic coarsening of the substrate. It effectively overprints the expected coarsening upward stacking pattern of a fill-and-spill setting.

The two contradictory trends in grain size with decreasing sill height can be related to different temporal and spatial scales. At the temporal and spatial scale of subsequent turbidites a fining upward stacking pattern is found. The autogenic coarsening of the substrate dominates the resulting depositional patterns at this scale. The model series with different initial sill heights represent a larger temporal and spatial scale of lobes or lobe complexes. At this scale the effects of flow stripping in a fill-and-spill basin are recognizable in the depositional characteristics of the turbidites. External processes determine the depositional pattern at this scale, because they act as a control on the recurrence interval of self-accelerating turbidity currents.

A conceptual model is presented to illustrate how the vertical grain size trends on the larger temporal and spatial scale depend on the sill height and the location in the ponded basin.

The inherent sensitivity of turbidity currents to substrate erodibility highlights the importance of further research in the field of turbidity current - bed interaction. Especially the effects of consolidation and cohesive forces on the erosion and entrainment rates demand more attention. However, both consolidation and cohesive forces remain difficult to scale in laboratory experiments. Numerical modelling approaches such as the one presented here, provide a useful tool in this further research.

Acknowledgements

I would like to thank my supervisors, Joris Eggenhuisen, Dirk-Jan Walstra, Joep Storms and Helena van der Vegt, for their continuous support, constructive discussions and comments on earlier versions. In addition, I would like to thank Dirk-Jan for the welcoming atmosphere at Deltares and Reinier Schrijvershof for helping me getting started with Delft3D so quickly. Furthermore, I want to thank Liang Li for helping with and providing some of the post-processing scripts. Without these, I would not have been able to extract from the data all the information I did. I really enjoyed the weekly group meetings at the TU Delft and found them very insightful. Finally, I want to thank Helena for her support and interest, not only regarding this thesis, but also regarding my further development and career.

References

Abd El-Gawad, S., Pirmez, C., Cantelli, A., Minisini, D., Sylvester, Z., and Imran, J. (2012). 3-D numerical simulation of turbidity currents in submarine canyons off the Niger Delta. *Marine Geology*, 326-328:55–66.

Al Ja'Aidi, O. S., McCaffrey, W. D., and Kneller, B. C. (2004). Factors influencing the deposit geometry of experimental turbidity currents: implications for sand-body architecture in confined basins. *Geological Society, London, Special Publications*, 222(1):45–58.

Altinakar, M., Graf, W., and Hopfinger, E. (1996). Flow structure in turbidity currents. *Journal of Hydraulic Research*, 34(5).

Amy, L. A., Kneller, B. C., and McCaffrey, W. D. (2007). Facies architecture of the Gres de Peira Cava, SE France: landward stacking patterns in ponded turbiditic basins. *Journal of the Geological Society*, 164(1):143–162.

Baas, J. H., van Kesteren, W., and Postma, G. (2004). Deposits of depletive high-density turbidity currents: A flume analogue of bed geometry, structure and texture. *Sedimentology*, 51(5):1053–1088.

Bagnold, R. A. (1954). Experiments on a gravity-free dispersion of large solid spheres in a Newtonian fluid under shear. In *Proceedings of the Royal Society of London A: Mathematical, Physical and Engineering Sciences*, volume 225, pages 49–63. The Royal Society.

Basani, R., Janocko, M., Cartigny, M. J. B., Hansen, E., and Eggenhuisen, J. T. (2014). MassFlOW-3D as a simulation tool for turbidity currents: some preliminary results. *International Association of Sedimentologists Special Publications*, 46(July):587–608.

Beaubouef, R. T. and Friedmann, S. J. (2000). High resolution seismic/ sequence stratigraphic framework for the evolution of Pleistocene intra slope basins, Western Gulf of Mexico: Depositional models and reservoir analogs. *GCSSEPM Foundation 20th Annual Research Conference, Deep-Water Reservoirs of the World*, (October):40–60.

Blanchette, F., Strauss, M., Meiburg, E., Kneller, B., and Glinsky, M. E. (2005). High-resolution numerical simulations of resuspending gravity currents: Conditions for self-sustainment. *Journal of Geophysical Research: Oceans*, 110(12):1–15.

Bolla Pittaluga, M. and Imran, J. (2014). A simple model for vertical profiles of velocity and suspended sediment concentration in straight and curved. *Journal of Geophysical Research: Earth Surface*, 119(3):483–503.

Brunt, R. L., McAffrey, W. D., and Kneller, B. C. (2004). Experimental Modeling of the Spatial Distribution of Grain Size Developed in a Fill-and-Spill Mini-Basin Setting. *Journal of Sedimentary Research*, 74(3):438–446.

Caldwell, R. L. and Edmonds, D. A. (2014). The effects of sediment properties on deltaic processes and morphologies: A numerical modeling study. *Journal of Geophysical Research: Earth Surface*, 119(5):961–982.

Cartigny, M. J. B., Eggenhuisen, J. T., Hansen, E. W. M., and Postma, G. (2013). Concentration-Dependent Flow Stratification In Experimental High-Density Turbidity Currents and Their Relevance To Turbidite Facies Models. *Journal of Sedimentary Research*, 83:1047–1065.

Commandeur, A. S. (2015). *Turbidity Currents in Reservoirs*. PhD thesis, Delft University of Technology.

de Leeuw, J., Eggenhuisen, J. T., and Cartigny, M. J. B. (2016). Morphodynamics of submarine channel inception revealed by new experimental approach. *Nature Communications*, 7:10886.

Deltares (2016). Delft3D-Flow User Manual.

Galappatti, G. and Vreugdenhil, C. B. (1985). A depth integrated model for suspended sediment transport. *Journal of Hydraulic Research*, 23(4):359–375.

Garcia, M. (1994). Depositional turbidity currents laden with poorly sorted sediment. *Journal of Hydraulic Engineering*, 120(11).

Geleynse, N., Storms, J. E. A., Walstra, D. J. R., Jagers, H. R. A., Wang, Z. B., and Stive, M. J. F. (2011). Controls on river delta formation; insights from numerical modelling. *Earth and Planetary Science Letters*, 302(1-2):217–226.

Grabowski, R., Droppo, I., and Wharton, G. (2011). Erodibility of cohesive sediment: The importance of sediment properties. *Earth-Science Reviews*, 105(3-4).

Hu, K., Ding, P., Wang, Z., and Yang, S. (2009). A 2D/3D hydrodynamic and sediment transport model for the Yangtze Estuary, China. *Journal of Marine Systems*, 77(1):114–136.

Hughes Clarke, J. (2016). First wide-angle view of channelized turbidity currents links migrating cyclic steps to flow characteristics. *Nature Communications*, 7.

Kneller, B. and Buckee, C. (2000). The structure and fluid mechanics of turbidity currents: a review of some recent studies and their geological implications. *Sedimentology*, 47:62–94.

Lesser, G. R., Roelvink, J. A., van Kester, J. A. T. M., and Stelling, G. S. (2004). Development and validation of a three-dimensional morphological model. *Coastal Engineering*, 51(8-9):883–915.

Mallarino, G., Beaubouef, R., Droxler, A., Abreu, V., and Labeyrie, L. (2006). Sea level influence on the nature and timing of a minibasin sedimentary fill (northwestern slope of the Gulf of Mexico). *AAPG Bulletin*, 90(7).

Meiburg, E. and Kneller, B. (2010). Turbidity Currents and Their Deposits. *Annual Review of Fluid Mechanics*, 42:135–156.

Meiburg, E., Radhakrishnan, S., and Nasr-Azadani, M. (2015). Modeling Gravity and Turbidity Currents: Computational Approaches and Challenges. *Applied Mechanics Reviews*, 67(4):040802.

Middleton, G. V. (1967). Experiments on density and turbidity currents: III. Deposition of sediment. *Canadian Journal of Earth Sciences*, 4(3):475–505.

Mitchener, H. and Torfs, H. (1996). Erosion of mud/sand mixtures. *Coastal Engineering*, 29(1-2):1–25.

Mutti, E. (1992). Turbidite sandstones: AGIP. *San Donato Milanese*.

Nikuradse, J. (1933). Gesetzmäßigkeiten der turbulenten Strömung in glatten Rohren (Nachtrag). *Forschung auf dem Gebiete des Ingenieurwesens*, 4(1).

Panagiotopoulos, I., Voulgaris, G., and Collins, M. (1997). The influence of clay on the threshold of movement of fine sandy beds. *Coastal Engineering*, 32(1).

Peakall, J., McCaffrey, B., and Kneller, B. (2000). A Process Model for the Evolution, Morphology, and Architecture of Sinuous Submarine Channels. *Journal of Sedimentary Research*, 70:434–448.

Postma, H. (1967). Sediment transport and sedimentation in the estuarine environment. *Estuaries*, 83:158–179.

Prather, B. E., Americas, S. U., Dairy, N., Road, A., Pirmez, C., and Winker, C. D. (2012). Stratigraphy of Linked Intraslope Basins : Brazos – Trinity System Western Gulf of Mexico. *SEPM Special publication*, (99):83–109.

Prélat, A., Hodgson, D., and Flint, S. (2009). Evolution, architecture and hierarchy of distributary deep-water deposits: a high-resolution outcrop investigation from the Permian Karoo Basin, South Africa. *Sedimentology*, 56(7).

Reading, H. and Richards, M. (1994). Turbidite systems in deep-water basin margins classified by grain size and feeder system. *American Association of Petroleum Geologists Bulletin*, 78(5):792–822.

Richardson, J. and Zaki, W. (1954). The sedimentation of a suspension of uniform spheres under conditions of viscous flow. *Chemical Engineering Science*, 3(2):65–73.

Romans, B. W., Normark, W. R., McGann, M. M., Covault, J. A., and Graham, S. A. (2009). Coarse-grained sediment delivery and distribution in the Holocene Santa Monica Basin, California: Implications for evaluating source-to-sink flux at millennial time scales. *Bulletin of the Geological Society of America*, 121(9-10):1394–1408.

Scheidegger, A. E. and Potter, P. E. (1971). Downcurrent decline of grain size and thickness of single turbidite beds: A semi-quantitative analysis. *Sedimentology*, 17(1-2):41–49.

Schuurman, F., Marra, W. A., and Kleinhans, M. G. (2013). Physics-based modeling of large braided sand-bed rivers: Bar pattern formation, dynamics, and sensitivity. *Journal of Geophysical Research: Earth Surface*, 118(4):2509–2527.

Sequeiros, O. E., Naruse, H., Endo, N., Garcia, M. H., and Parker, G. (2009). Experimental study on self-accelerating turbidity currents. *Journal of Geophysical Research*, 114(C5):C05025.

Sinclair, H. D. and Tomasso, M. (2002). Depositional Evolution of Confined Turbidite Basins. *Journal of Sedimentary Research*, 72(4):451–456.

Straub, K. M., Mohrig, D., McElroy, B., Buttles, J., and Pirmez, C. (2008). Interactions between turbidity currents and topography in aggrading sinuous submarine channels: A laboratory study. *Bulletin of the Geological Society of America*, 120(3-4):368–385.

Traer, M. M., Hilley, G. E., Fildani, A., and McHargue, T. (2012). The sensitivity of turbidity currents to mass and momentum exchanges between these underflows and their surroundings. *Journal of Geophysical Research: Earth Surface*, 117(1):1–16.

van der Vegt, H., Storms, J., Walstra, D., and Howes, N. (2016). Can bed load transport drive varying depositional behaviour in river delta environments? *Sedimentary Geology*, 345:19–32.

van Maren, D. (2007). Grain size and sediment concentration effects on channel patterns of silt-laden rivers. *Sedimentary Geology*, 202(1):297–316.

Van Rijn, L., Nieuwjaar, M., van der Kaay, T., Nap, E., and van Kampen, A. (1993). Transport of fine sands by currents and waves. *Journal of Waterway, Port, Coastal and Ocean Engineering*, 119(2).

van Rijn, L. C. (2007a). Unified View of Sediment Transport by Currents and Waves. I: Initiation of Motion, Bed Roughness, and Bed-Load Transport. *Journal of Hydraulic Engineering*, 133(6):649–667.

van Rijn, L. C. (2007b). Unified View of Sediment Transport by Currents and Waves. II: Suspended Transport. *Journal of Hydraulic Engineering*, 133(6):668–689.

van Rijn, L. C. (2007c). Unified View of Sediment Transport by Currents and Waves. III: Graded Beds. *Journal of Hydraulic Engineering*, 133(7):761–775.

Violet, J., Sheets, B., Pratson, L., Paola, C., Beaubouef, R., and Parker, G. (2005). Experiment on Turbidity Currents and Their Deposits in a Model 3D Subsiding Minibasin. *Journal of Sedimentary Research*, 75(5):820–843.

Weimer, P. and Slatt, R. M. (2007a). Introduction to Deepwater Systems. In *Petroleum Geology of Deepwater Settings*, chapter 1, pages 1–18. AAPG/Datapages.

Weimer, P. and Slatt, R. M. (2007b). Overview of Deepwater-Reservoir Elements. In *Petroleum Geology of Deepwater Settings*, chapter 5, pages 149–170. AAPG/Datapages.

Winker, C. D. (1996). High-resolution seismic stratigraphy of a late Pleistocene submarine fan ponded by salt-withdrawal mini-basins on the Gulf of Mexico continental slope. In *Proceedings of the Annual Offshore Technology Conference*, volume 1.

Xu, J. P. (2010). Normalized velocity profiles of field-measured turbidity currents. *Geology*, 38(6):563–566.